REPORT 1031

A STUDY OF THE USE OF EXPERIMENTAL STABILITY DERIVATIVES IN THE CALCULATION OF THE LATERAL DISTURBED MOTIONS OF A SWEPT-WING AIRPLANE AND COMPARISON WITH FLIGHT RESULTS [1]

By JOHN D. BIRD and BYRON M. JAQUET

SUMMARY

An investigation was made to determine the accuracy with which the lateral flight motions of a swept-wing airplane could be predicted from experimental stability derivatives determined in the 6-foot-diameter rolling-flow test section and 6- by 6-foot curved-flow test section of the Langley stability tunnel. In addition determination of the significance of including the nonlinear aerodynamic effects of sideslip in the calculations of the motions was desired. All experimental aerodynamic data necessary for prediction of the lateral flight motions are presented along with a number of comparisons between flight and calculated motions caused by rudder and aileron disturbances.

In general, the agreement between the calculated and measured motions of the airplane considered was good when the effects of all control movements were taken into account. The greatest disagreement occurred at lift coefficients where Reynolds number effects on the experimental derivatives would be expected to be high, which for the case considered was for lift coefficients above about 0.8 when wing slots were used. The nonlinear effects of sideslip for this airplane were not very significant for the motions considered, which generally involved sideslip angles less than 10°.

INTRODUCTION

For the past few years, numerous investigations have been made in the Langley stability tunnel to determine the effects of geometric variables on the static-, rolling-, yawing-, and pitching-stability derivatives of various airplane configurations. (See references 1 to 4.) In the past, however, none of the experimental data have been compared with data obtained in flight to determine its relative worth. The purpose of the present report is to determine the applicability of the experimental stability derivatives to the prediction of the lateral disturbed motions of an airplane in flight. The equations used for calculating the motions are given in the appendix.

A ⅛-scale model of a swept-wing version of a conventional fighter airplane, which was selected because of the large amount of flight data available (see references 5 and 6), was tested in the 6-foot-diameter rolling-flow test section and 6- by 6-foot curved-flow test section of the Langley stability tunnel to determine all the stability derivatives which are usually considered necessary to calculate the lateral motions arising from a disturbance caused by the rudder or the ailerons. Comparisons have been made between the flight and calculated lateral motions for a wide range of conditions in gliding flight.

A few calculations have been made to determine the effects of nonlinear variations of the aerodynamic forces and moments with the angle of sideslip.

COEFFICIENTS AND SYMBOLS

The results of the wind-tunnel tests are presented as standard NACA coefficients of forces and moments. Moment coefficients are referred to a center of gravity located at 21.8 percent of the mean aerodynamic chord. The wind-tunnel data and motion calculations are referred to the stability axes, which are a system of axes having their origin at the center of gravity and in which the Z-axis is in the plane of symmetry and perpendicular to the relative wind, the X-axis is in the plane of symmetry and perpendicular to the Z-axis, and the Y-axis is perpendicular to the plane of symmetry. The positive directions of the stability axes and of angular displacements of the airplane and control surfaces are shown in figure 1.

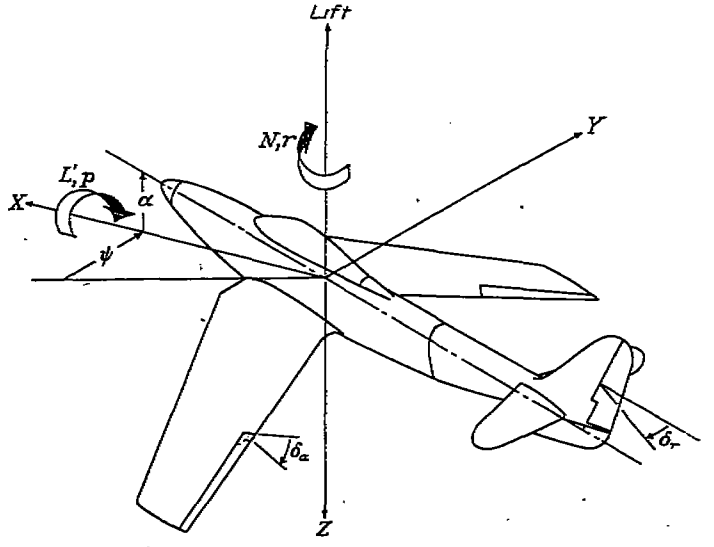

FIGURE 1.—System of stability axes. Arrows indicate positive forces, moments, and angular displacements.

[1] Supersedes NACA TN 2013, "A Study of the Use of Experimental Stability Derivatives in the Calculation of the Lateral Disturbed Motions of a Swept-Wing Airplane and Comparison with Flight Results" by John D. Bird and Byron M. Jaquet, 1950.

The coefficients and symbols are defined as follows:

C_L	lift coefficient (Lift $/qS$)
$C_{L_{max}}$	maximum lift coefficient
C_X	longitudinal-force coefficient (X/qS)
C_Y	lateral-force coefficient (Y/qS)
C_l	rolling-moment coefficient (L/qSb)
C_n	yawing-moment coefficient (N/qSb)
$C_{Y_\psi}=\frac{\partial C_Y}{\partial \psi}$	
$C_{l_\psi}=\frac{\partial C_l}{\partial \psi}$	
$C_{n_\psi}=\frac{\partial C_n}{\partial \psi}$	
$C_{l_\beta}=\frac{\partial C_l}{\partial \beta}$	
$C_{n_\beta}=\frac{\partial C_n}{\partial \beta}$	
$C_{Y_p}=\frac{\partial C_Y}{\partial \frac{pb}{2V}}$	
$C_{l_p}=\frac{\partial C_l}{\partial \frac{pb}{2V}}$	
$C_{n_p}=\frac{\partial C_n}{\partial \frac{pb}{2V}}$	
$C_{Y_r}=\frac{\partial C_Y}{\partial \frac{rb}{2V}}$	
$C_{l_r}=\frac{\partial C_l}{\partial \frac{rb}{2V}}$	
$C_{n_r}=\frac{\partial C_n}{\partial \frac{rb}{2V}}$	
I_{X_0}	moment of inertia about longitudinal principal axis
I_{Y_0}	moment of inertia about spanwise principal axis
I_{Z_0}	moment of inertia about normal principal axis
X	longitudinal force along X-axis
Y	lateral force along Y-axis
Z	normal force along Z-axis (Lift$=-Z$)
L	rolling-moment about X-axis
N	yawing-moment about Z-axis
$pb/2V$	wing-tip helix angle, radians
$rb/2V$	yawing-velocity parameter, radian measure
p	rolling angular velocity about X-axis
r	yawing angular velocity about Z-axis
v	linear velocity of airplane along Y-axis
V	free-stream velocity along X-axis
V_c	calibrated airspeed, based on sea-level density of air
β	angle of sideslip; $\beta=-\psi$ in wind-tunnel tests $\left(\tan^{-1}\frac{v}{V}\right)$
α_R	angle of attack of wing root chord line
α	angle of attack of thrust line ($\alpha_R-1.2°$)
ψ	angle of yaw, degrees
i_t	angle of incidence of stabilizer with respect to thrust line, positive when trailing edge is down
δ	control-surface deflection, measured in a plane perpendicular to hinge axis
Λ	angle of sweepback, degrees
q	free-stream dynamic pressure $\left(\frac{1}{2}\rho V^2\right)$
S	wing area
b	wing span
A	aspect ratio (b^2/S)
ρ	mass density of air
T	time
$T_{1/2}$	time to damp to half amplitude
P	period
l	tail length

Subscripts:

a	aileron
r	rudder
f	flap
v	vertical tail

WIND-TUNNEL TESTS

APPARATUS AND MODEL

The experimental static-lateral-stability derivatives, rolling-stability derivatives, and yawing-stability derivatives were determined from tests conducted in the Langley stability tunnel in which rolling or curved flight is simulated by rolling or curving the air stream about a rigidly mounted model.

The tests were made on a conventional six-component balance system with the model mounted at the flight center of gravity which is at 21.8 percent of the mean aerodynamic chord of the wing.

The full-scale airplane (a swept-wing version of a conventional fighter) had the quarter-chord line of the wing, just outboard of the intake ducts, swept back 35°. Some of the pertinent airplane characteristics are given in table I. More details of the airplane may be obtained from references 5 and 6.

The $\frac{1}{9}$-scale model shown in figure 2 and in the photographs of figures 3 to 6 was constructed of laminated mahogany, finished in clear lacquer, and all surfaces were highly polished. The model propeller had three metal blades set at an angle of 28° at the 0.75 radius. All propeller-on tests were made with windmilling propeller. The model wing had a removable leading edge so that slats of 0 percent, 40 percent, and 80 percent of the swept span could be used interchangeably to simulate those of the full-scale airplane. The top surfaces of the slats were cast to the contour of the airfoil and the slats were extended by means of metal brackets which also act as fences to reduce spanwise flow along the slot. A cross section through the slot and slat is shown in reference 5.

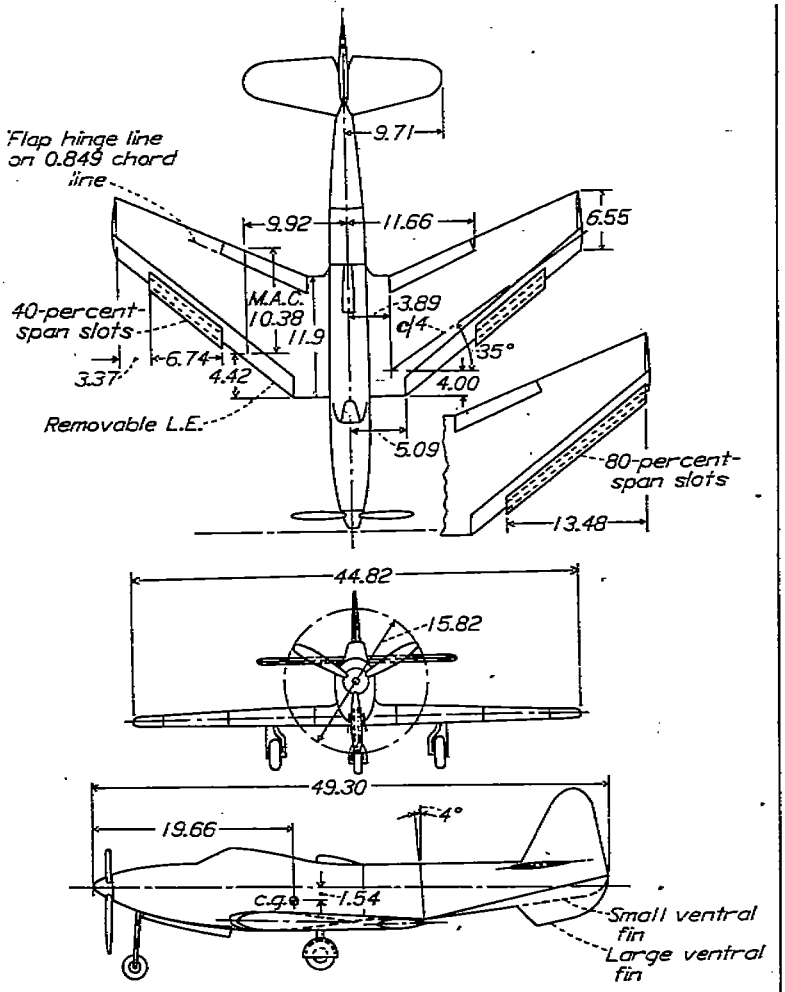

FIGURE 2.—Geometric characteristics of 1/6-scale model of test airplane. All dimensions are in inches.

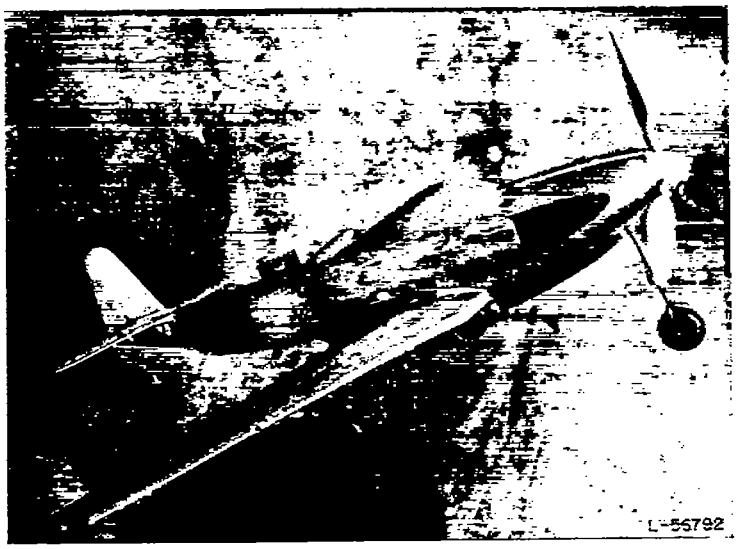

FIGURE 3.—Side view of 1/6-scale model mounted in 6-foot-diameter rolling-flow test section of Langley stability tunnel.

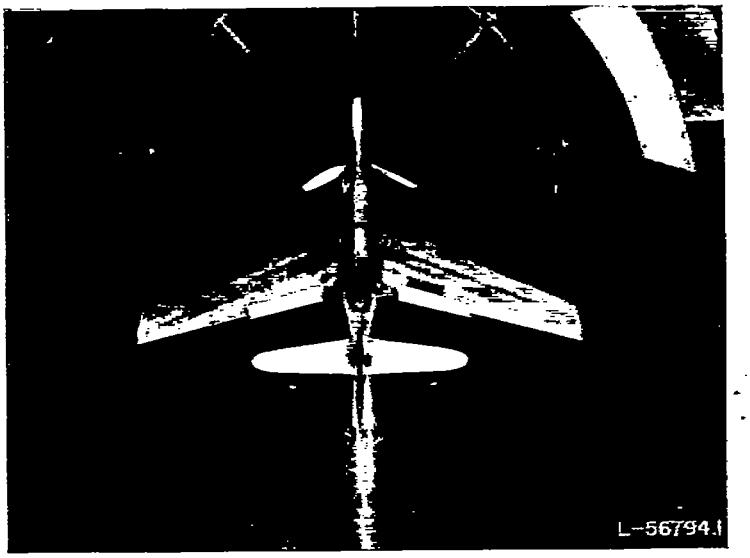

FIGURE 4.—Rear view of 1/6-scale model mounted in 6-foot-diameter rolling-flow test section of Langley stability tunnel.

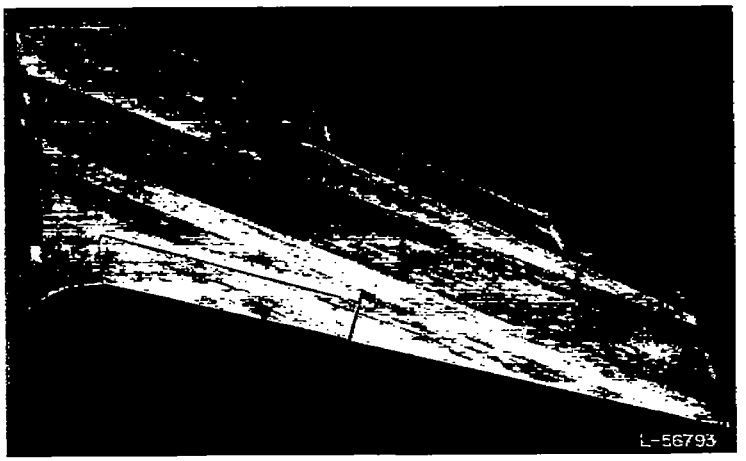

FIGURE 5.—Close-up of 40-percent leading-edge slots on 1/6-scale model.

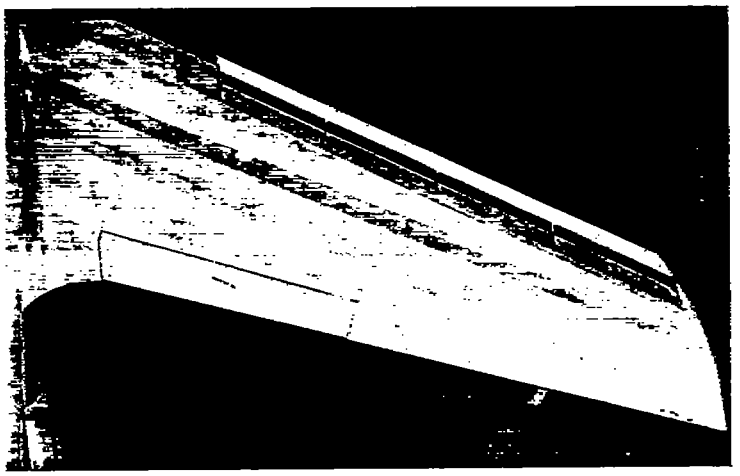

FIGURE 6.—Close-up of 80-percent leading-edge slots on 1/6-scale model.

The wing had a plain trailing-edge flap with a chord of 15.1 percent of the wing chord measured perpendicular to the hinge axis. The gap was sealed for all tests. As in the case of the airplane the main wheels of the model were fixed for all tests; whereas the nose wheel and nose-wheel doors were removed for all flaps-up tests.

Shown in figure 2 are the two ventral fins tested on the model. The large ventral fin was used for all tests except a few with the 80-percent-span slot configuration for which the small ventral fin was used.

TEST AND TEST CONDITIONS

Trim tests.—Model trim lift coefficients of 0.33, 0.55, 0.76, and 0.95 were selected as representative of those obtained in flight tests. The angle of incidence of the horizontal tail was measured with respect to the thrust line.

In order to determine the trim angles of the horizontal tail for the previously mentioned lift coefficients, tests were made through the angle-of-attack range with the horizontal tail set at $-5°$, $-3°$, and $1°$ incidence. From these tests the trim angles of the horizontal tail were determined. (See table II.)

Static tests.—In order to determine the static-stability derivatives C_{l_ψ}, C_{n_ψ}, and C_{Y_ψ}, the model was tested at $\psi=\pm5°$ through an angle-of-attack range of $\alpha=-2°$ to $\alpha=23°$ for the flaps up (trim $C_L=0.33$) and $\alpha=-2°$ to $\alpha=18°$ for the flaps down (trim $C_L=0.76$) for each of the slot configurations. Tests were also made at all selected test trim lift coefficients through an angle-of-yaw range of $\psi=\pm20°$ to determine the variations of C_l, C_n, and C_Y with ψ for all slot configurations.

Tare tests were made for the 40-percent-span slot configuration (flaps up and down). The effect of the slots on the tares was assumed to be small; therefore, the tares for the 40-percent-span slot configuration were applied to all configurations. The Mach and Reynolds numbers for the tests were 0.17 and 1.01×10^6, respectively.

Rolling-flow tests.—Tests were conducted in the 6-foot-diameter rolling-flow test section of the Langley stability tunnel, wherein rolling flight of the model was simulated by rotating the air stream. The model was mounted rigidly on a conventional support strut. Details of this test procedure are given in reference 1.

All slot configurations were tested through the angle-of-attack range with the flaps up (trim $C_L=0.33$) and with the flaps down (trim $C_L=0.76$) at helix angles $pb/2V$ of 0, ±0.0253, and ±0.0757 radian. The slopes of C_l, C_n, and C_Y plotted against $pb/2V$ are the derivatives C_{l_p}, C_{n_p}, and C_{Y_p}. The 40-percent-span slot configuration (flaps up and down) was tested at the selected trim lift coefficients for the previously mentioned values of $pb/2V$ from $\psi=0°$ to $\psi=20°$ to determine the variation of C_{l_p}, C_{n_p}, and C_{Y_p} with ψ. The Mach number and Reynolds number for the rolling-flow tests were 0.17 and 1.01×10^6, respectively.

Yawing-flow tests.—Yawing-flow tests were conducted in the 6- by 6-foot curved-flow test section of the Langley stability tunnel. In this section, curved flight is simulated approximately by directing the air in a curved path about a fixed model.

All slot configurations were tested in curved flow through the angle-of-attack range with the flaps up (trim $C_L=0.33$) and with the flaps down (trim $C_L=0.76$) at values at $rb/2V$ of 0, -0.039, -0.082, and -0.108. The slopes of C_l, C_n, and C_Y plotted against $rb/2V$ are the derivatives C_{l_r}, C_{n_r}, and C_{Y_r}.

The 40-percent-span slot configuration (flaps up and down) was tested through an angle-of-yaw range of $\psi=\pm20°$ for values of $rb/2V$ of 0, -0.039, -0.082, and -0.108 at the previously mentioned trim lift coefficients to determine the variation of C_{l_r}, C_{n_r}, and C_{Y_r} with ψ. The values presented herein are the average of the results at corresponding positive and negative angles of yaw.

The 40-percent-span slot configuration (flaps up) was tested at a trim lift coefficient of 0.33 through the angle-of-yaw range with the propeller off.

The yawing-flow tests were made at a Mach number of 0.13 and a Reynolds number of 0.8×10^6.

CORRECTIONS

Approximate jet-boundary corrections based on methods derived for unswept wings were applied to the angle of attack, longitudinal-force coefficient, and rolling-moment coefficient, and a blocking correction of 1.01 was applied to the dynamic pressure.

Corrections for the effect of the support strut have been applied to C_X, C_L, C_l, C_n, C_Y, C_{l_ψ}, C_{n_ψ}, and C_{Y_ψ}. In rolling flow and curved flow, accurate tares were difficult to obtain; and, as a result, the derivatives C_{l_p}, C_{n_p}, C_{Y_p}, C_{l_r}, C_{n_r}, and C_{Y_r} are not corrected for the effects of the support strut.

The derivative C_{l_p} was corrected for the effective pitching velocity, which exists when the model is tested at an angle of yaw, by the following equation:

$$C_{l_p}=C_{l_p}'\cos\psi+f(A,\Lambda,\psi)$$

where C_{l_p}' is measured about the wind axis, and $f(A,\Lambda,\psi)$, which is small as compared with $C_{l_p}'\cos\psi$, is a function determined by use of the methods of reference 4. Corresponding effective pitching corrections were not applied to the derivatives C_{n_p} and C_{Y_p}.

A correction was also applied to the derivative C_{Y_r} to account for the error caused by the cross-tunnel static-pressure gradient which is associated with curved flow.

EXPERIMENTAL RESULTS

The experimental data are discussed briefly with reference to the effects of the slots and angle of yaw on the aerodynamic characteristics of the model, because the effects of these variables on the rotary derivatives have not been investigated extensively to date. The figures which present the results obtained in the present investigation are listed in table III.

The basic lift and longitudinal-force data of figures 7 and 8 are generally in good agreement with larger scale tests of another model of the same airplane, as given in reference 7.

The main effect of the slots is to extend the linear range of those stability derivatives which are largely contributed by the wing to higher lift coefficients in a manner similar to the effect of slots on the lift curve of a wing. (See figs. 7 to 10 and 12, 13, 15, and 16.) One significant effect of the slots is on the damping in yaw C_{n_r} which increased as the slot span is increased. When the 80-percent-span slots are used C_{n_r} is increased (over that of the unslotted configuration) by about 25 percent at $C_L=0$. (See fig. 15 (a).) When the flaps are deflected (fig. 15 (b)), the effects of the slots on the yawing-stability derivatives are not as great as when the flaps are retracted.

A comparison of figures 11(a) to 11(f) shows that C_{n_ψ} varies to some extent through the yaw range, C_{Y_ψ} is approximately constant, and for any given lift coefficient C_{l_ψ} is approximately constant between $\psi=-10°$ and $\psi=10°$. As the angle of yaw is increased (fig. 14 (a)), C_{Y_p} tends to decrease, C_{n_p} remains approximately constant, and C_{l_p} decreases slightly. The variations are similar when the flaps are deflected. (See fig. 14 (b).)

The tests for the determination of the variation of C_{Y_r}, C_{n_r}, and C_{l_r} with ψ were made for negative values of $rb/2V$ only. Results for positive values of $rb/2V$ and positive ψ were obtained by assuming that the model was essentially symmetrical about the XZ-plane and by utilizing the results for the corresponding opposite angles of yaw and $rb/2V$ with regard for signs. This procedure amounted to averaging the derivatives for corresponding positive and negative angles of yaw.

In general, as the angle of yaw is increased from 0° to 20°, the damping in yaw C_{n_r} is increased by about 15 percent, and C_{Y_r} and C_{l_r} are decreased slightly (fig. 17 (a)). Deflection of the flaps or removal of the propeller does not appreciably

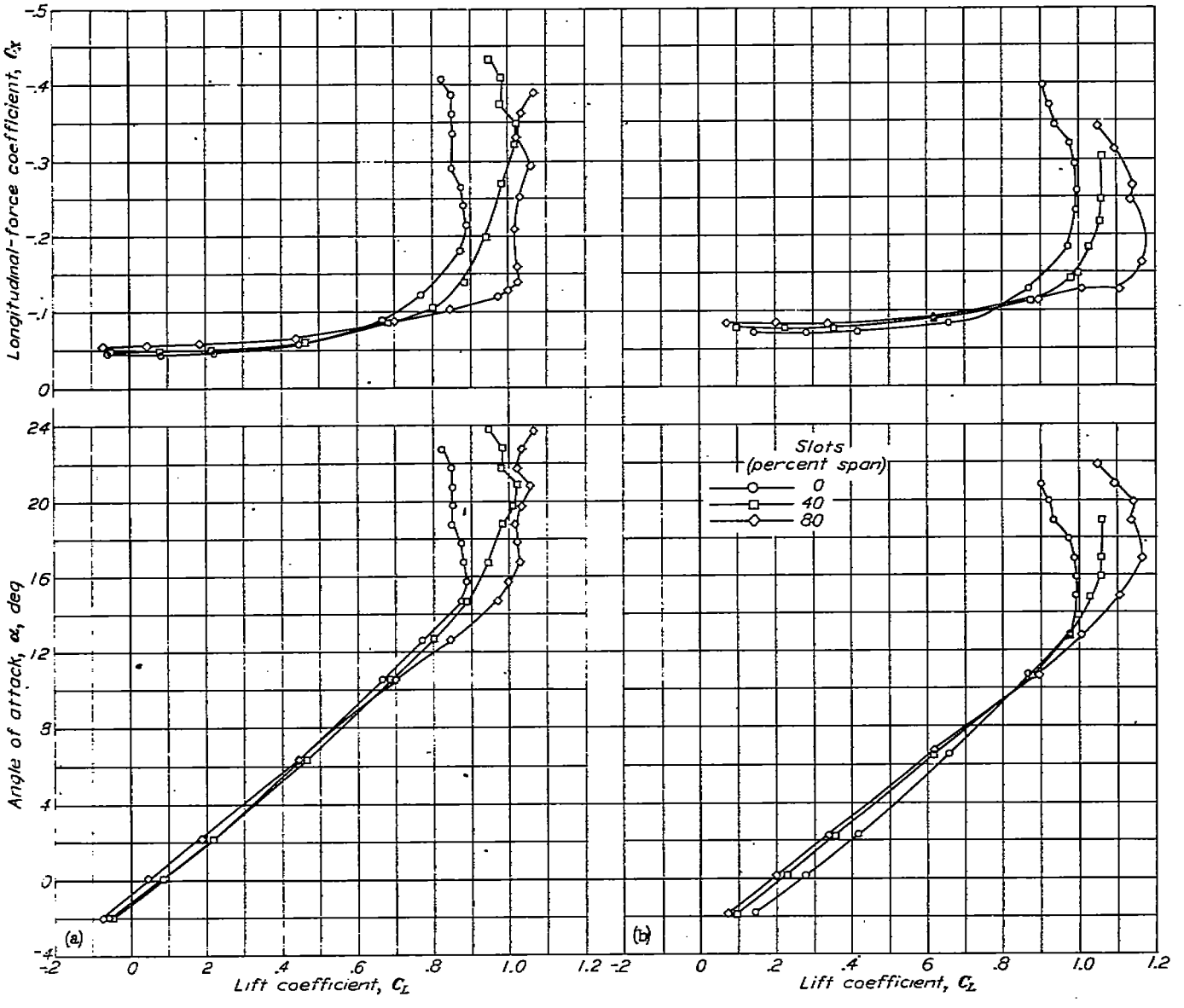

(a) Trim $C_L=0.33$; $\delta_f=0°$.

(b) Trim $C_L=0.76$; $\delta_f=40°$.

FIGURE 7.—Variation of longitudinal-force coefficient and angle of attack with lift coefficient for three slot configurations. Large ventral fin on; propeller on; $\psi=0°$; $R=1.01\times10^6$.

change the variations of the yawing-stability derivatives with angle of yaw. (See fig. 17.)

Because C_{n_r} is largely dependent on the size of the vertical tail it is approximately true throughout the yaw range that

$$C_{n_r}=-\frac{2l_t}{b}C_{n_{\beta_v}}$$

Substitution of the proper values of the span, $C_{n_{\beta_v}}$, and the tail length l_t indicates that the trend of the variation of C_{n_r} with ψ shown in figure 17 is reasonable.

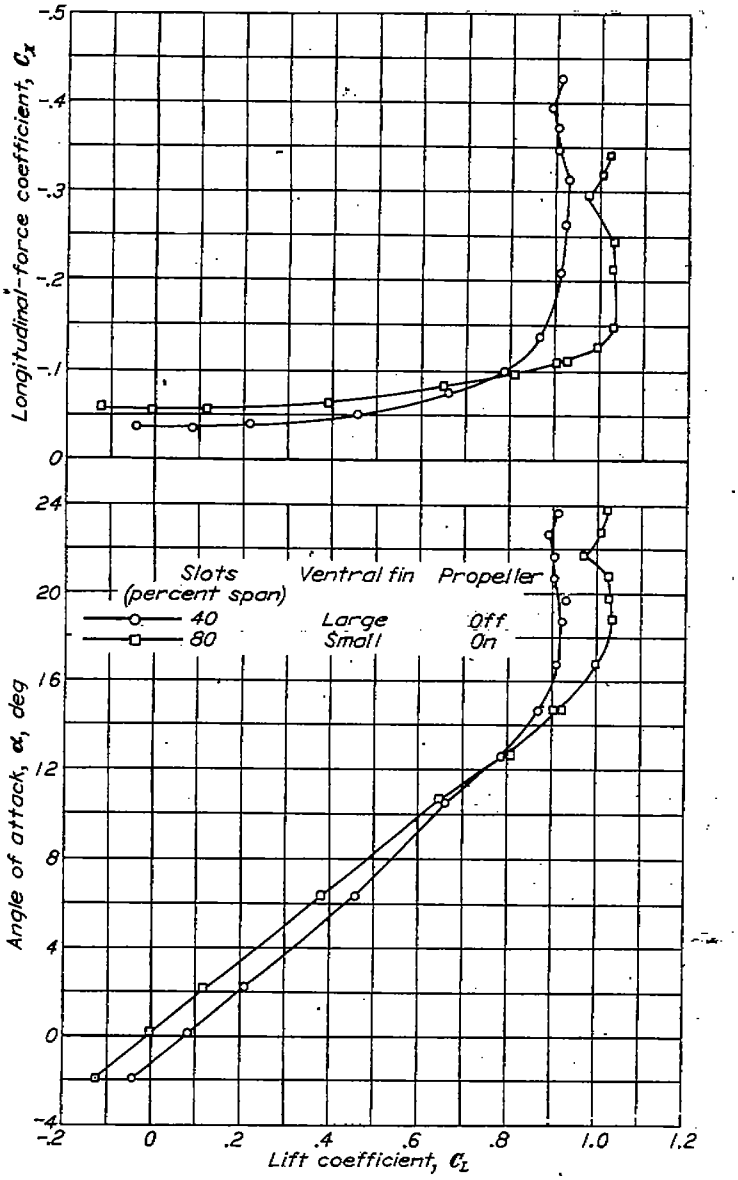

FIGURE 8.—Variation of longitudinal-force coefficient and angle of attack with lift coefficient for two slot configurations. Trim C_L=0.33; ψ=0°; δ_f=0°; R=1.01×10⁶.

The relative constancy of C_{Y_p}, C_{l_p}, C_{n_p}, C_{Y_r}, C_{l_r}, and C_{n_r} with angle of yaw as indicated by figures 14 and 17 and the linearity of the curves of C_Y, C_l, and C_n plotted against ψ for angles of yaw up to approximately 10° (fig. 11) were factors which indicated that nonlinearities were not of first-order importance for this airplane in the calculation of motions involving reasonably small variations in ψ. Consequently, most of the motion calculations neglect the effect of ψ on the stability derivatives.

The results of unpublished tests of swept wings at Reynolds numbers to 8.0×10^6 in the Langley 19-foot pressure tunnel indicate that the linear part of the curve of C_{l_ψ} plotted against C_L is increased by an increase in Reynolds number. The curves of C_{l_ψ} against C_L given herein agree well with those obtained in flight (references 5 and 6) and in tests of a $\frac{1}{4.5}$-scale model (reference 7) except at lift coefficients above C_L=0.8 where the magnitude of the present test values decreases for the slotted-wing configurations. The linear parts of the curves of the rolling- and yawing-stability derivatives are believed to be extended similarly to higher lift coefficients if the Reynolds number is increased.

MOTION CALCULATION METHODS

The lateral disturbed motions of the test airplane were calculated from the aerodynamic data obtained from the tests described in the section entitled "Wind-Tunnel Tests." The mass and dimensional characteristics of the airplane are given in table I, and a tabulation of the flight conditions for which lateral disturbed motions were calculated for comparison with the flight motions is given in table IV. Most of the calculations involved dynamic derivatives which were constant for a given lift coefficient as is usually employed in the theory of small disturbances used in lateral-stability calculations.

Solutions of the lateral equations of motion, given in the appendix, were obtained for unit step disturbances in roll and yaw by the method described in reference 8. The aileron and rudder deflections during the flight motion under investigation were then approximated by a series of step functions usually at $\frac{1}{2}$-second intervals. The motion arising from the control movements was then calculated by

$$\beta_n,\ p_n,\ \text{or}\ r_n=\sum_{n=0}^{m}\left[(\delta_{m-n})_{rudder}(B_n)_{yaw}+(\delta_{m-n})_{aileron}(B_n)_{roll}\right]$$

where B_n is the value of the unit solution caused by $\Delta C_n'=1$ or $\Delta C_l=1$ at a time $T=kn$, and δ_{m-n} is the fraction of the unit disturbance applied by the rudder or aileron at a time $T=k(m-n)$. The rudder and aileron effectiveness were

obtained from reference 7. This procedure is essentially an approximate evaluation of Duhamel's integral and was considered sufficiently accurate for these calculations. Reference 8 gives a more exact graphical evaluation of this integral. The yawing moment caused by aileron deflection and the rolling moment caused by rudder deflection were not considered of enough significance to warrant their inclusion in these calculations. In some cases, however, these factors may be of greater significance.

In a few cases, unit solutions to the equations of motion were obtained by a Laplace transform procedure which has been adapted for use with automatic digital computers. The results were, of course, identical with those presented in this report.

Calculations of the lateral motions for a few cases employing a nonlinear variation of rolling-moment and yawing-moment coefficients with angle of sideslip and a variation of C_{n_r} with angle of sideslip were carried out by use of the Kutta three-eighths rule for solving the lateral equations of motion. (See reference 9.) All lateral-motion calculations were made on an automatic digital computing machine.

CALCULATED LATERAL MOTIONS

GENERAL

The flight records corresponding to the motions calculated for this report showed that the motions resulting from right and left control movements were not exactly of opposite magnitude. This result indicates that there was some asymmetry in the characteristics of the airplane, although the

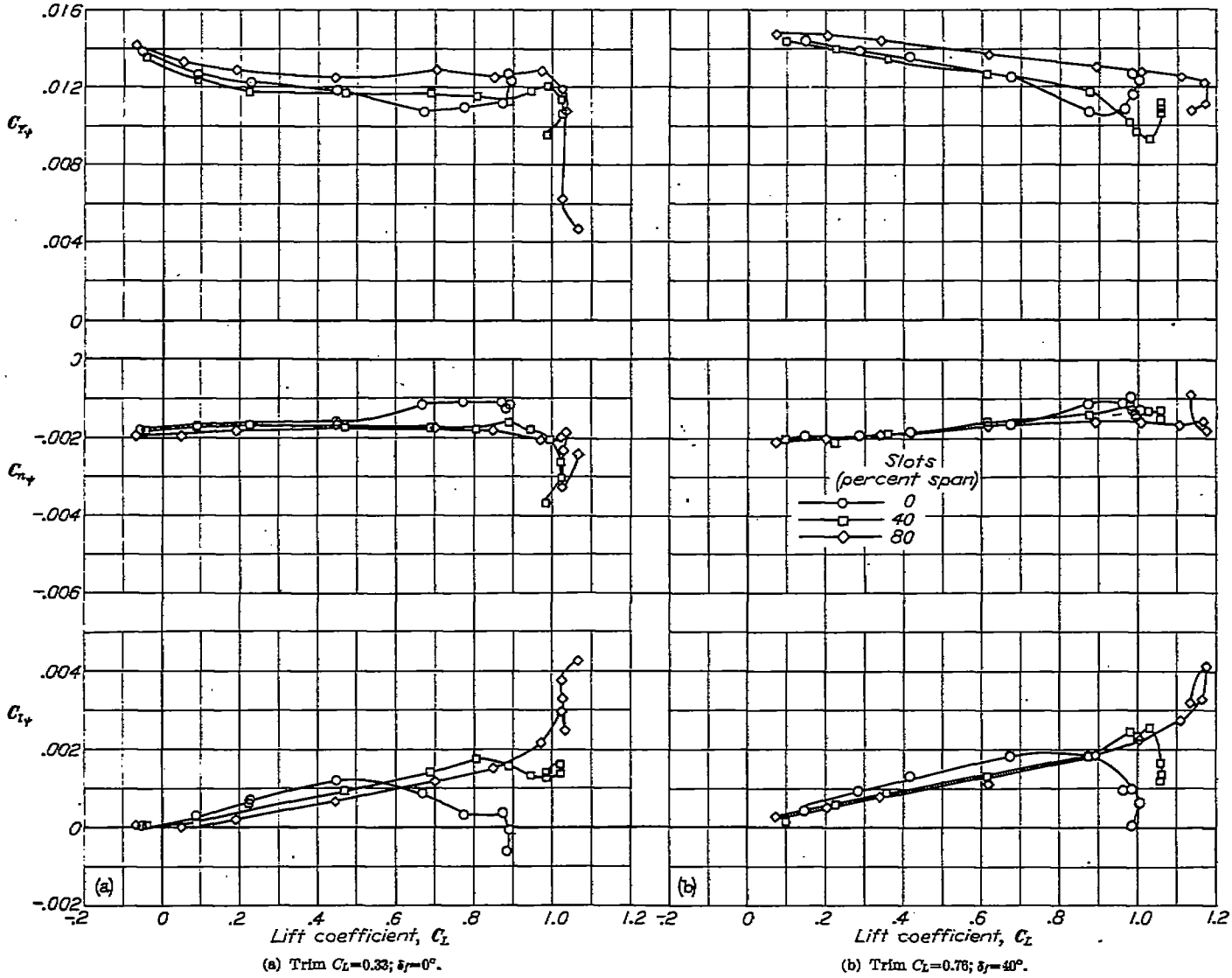

(a) Trim C_L=0.33; δ_f=0°. (b) Trim C_L=0.76; δ_f=40°.

FIGURE 9.—Variation of lateral static-stability derivatives with lift coefficient for three slot configurations. Large ventral fin on; propeller on; ψ=0°; R=1.01×10^6.

wind-tunnel test results indicated no marked asymmetry in the model characteristics. Part of the differences in the flight motions to the right and left are undoubtedly due to variation in the thrust conditions. Although the flight tests were made under approximately zero thrust, no convenient means of obtaining this condition was available, and thus this requirement was left to the judgement of the pilot. Some small part of the difference in the motions to the left and right should be attributable to instrument error as the film record frequently contained considerable hash which, of course, tended to obscure the actual motion record. The differences between the motions to the right and left were resolved in the present report by presenting both records with the sign of one reversed so that the motions were superimposed. The shaded areas in the lateral-motion plots (figs. 18 to 23 and 25 to 35) represent the difference between the motions to the right and left. The flight motions corresponding to the calculated motions were obtained from references 5 and 6 and related tests. The figures which present the results of the lateral-motion calculations are listed in table III.

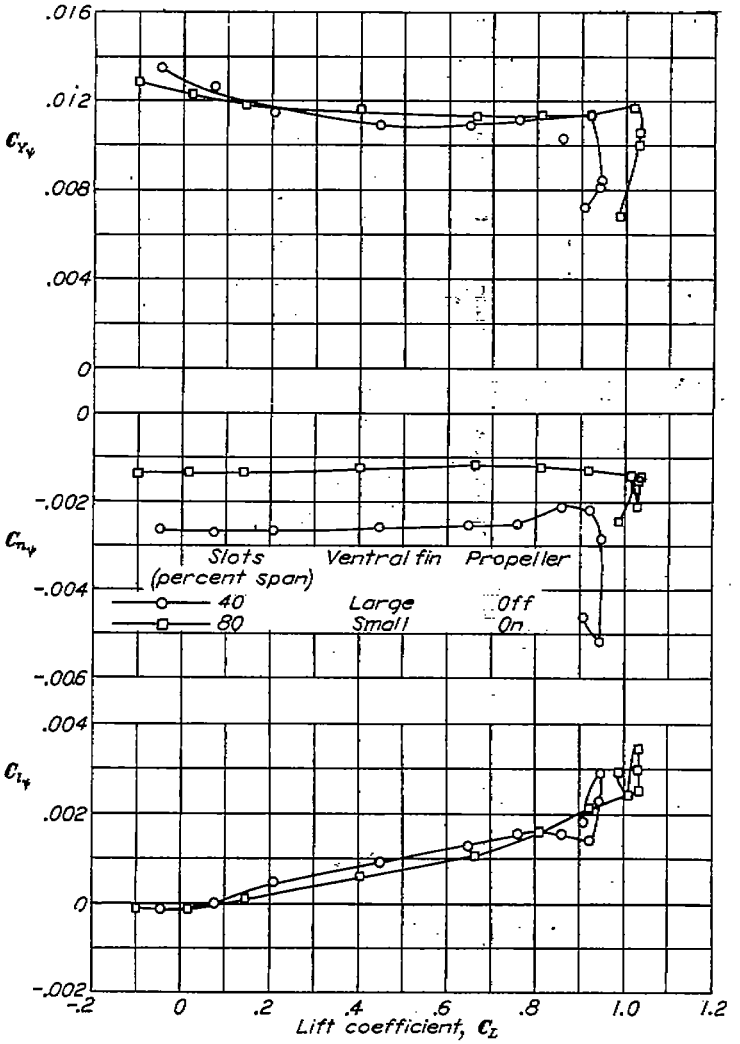

FIGURE 10.—Variation of lateral static-stability derivatives with lift coefficient for two slot configurations. Trim C_L=0.33; ψ=0°; δ_f=0°; R=1.01×10⁶.

LATERAL OSCILLATIONS

Lateral oscillations were initiated by abruptly deflecting the rudder of the airplane and returning it to neutral equally as rapid a moment later. Some aileron waggle caused by the floating tendency of the ailerons occurred and was accounted for in the calculations by the procedure given in the calculation methods.

The calculated and flight motions are generally in good agreement for all motions calculated (figs. 18 to 23) except for the condition at C_L=0.977. (See fig. 23.) A comparison of the flight and calculated periods and time to damp to half amplitude (fig. 24) also indicate fairly good agreement except for the motions at lift coefficients of 0.977 and 1.169.

The values of C_{l_β} used for the calculation of the lateral motions were obtained from the curves of C_l plotted against ψ (fig. 11) wherever possible rather than the curves of C_{l_ψ} obtained from tests made at $\psi=\pm 5°$ (figs. 9 and 10) because this procedure is believed to be more accurate. Although the difference between the two methods is generally small, such is not always true; and in some cases the calculated rate of damping was found to be appreciably affected by the difference in C_{l_β}.

At the higher lift coefficients, the experimental stability derivatives deviate appreciably from their initial trends. This tendency previously has been referred to as a Reynolds number effect and is probably the cause for the lack of agreement at high lift coefficients between the flight and calculated results. References 5 and 6 which present flight tests for this airplane show no reduction in C_{l_ψ} up to the maximum test lift coefficient. The rotary derivatives of the airplane presumably behave similarly. Evidence of the deviation of the experimental stability derivatives from their true variation with lift coefficient is observed in figure 20 which presents results for a lateral oscillation occurring at C_L=0.759. The calculated result indicates an excessive response in sideslip, yaw, and roll.

A few additional calculations of the period and time to damp, made for other high lift coefficients in flight, indicate increasingly poor agreement between the flight and calculated times to damp to one-half amplitude with increasing lift coefficient. The relatively good agreement between the periods of the flight and calculated motions for all lift coefficients, however, indicates that the experimental values of C_{n_β} are fairly close to the correct values. The period of the motion is primarily a function of the directional-stability parameter C_{n_β}. (See reference 10.) An extrapolation of the curves of the derivatives plotted against lift coefficient—which amounted to selecting the value of the derivative just previous to the break in the curves occurring at maximum lift coefficient—was employed for one case at C_L=1.17 but failed to yield a satisfactory result. A linear extrapolation of the curves in the region preceding the departure from the theoretical or linear trend is expected to be more satisfactory.

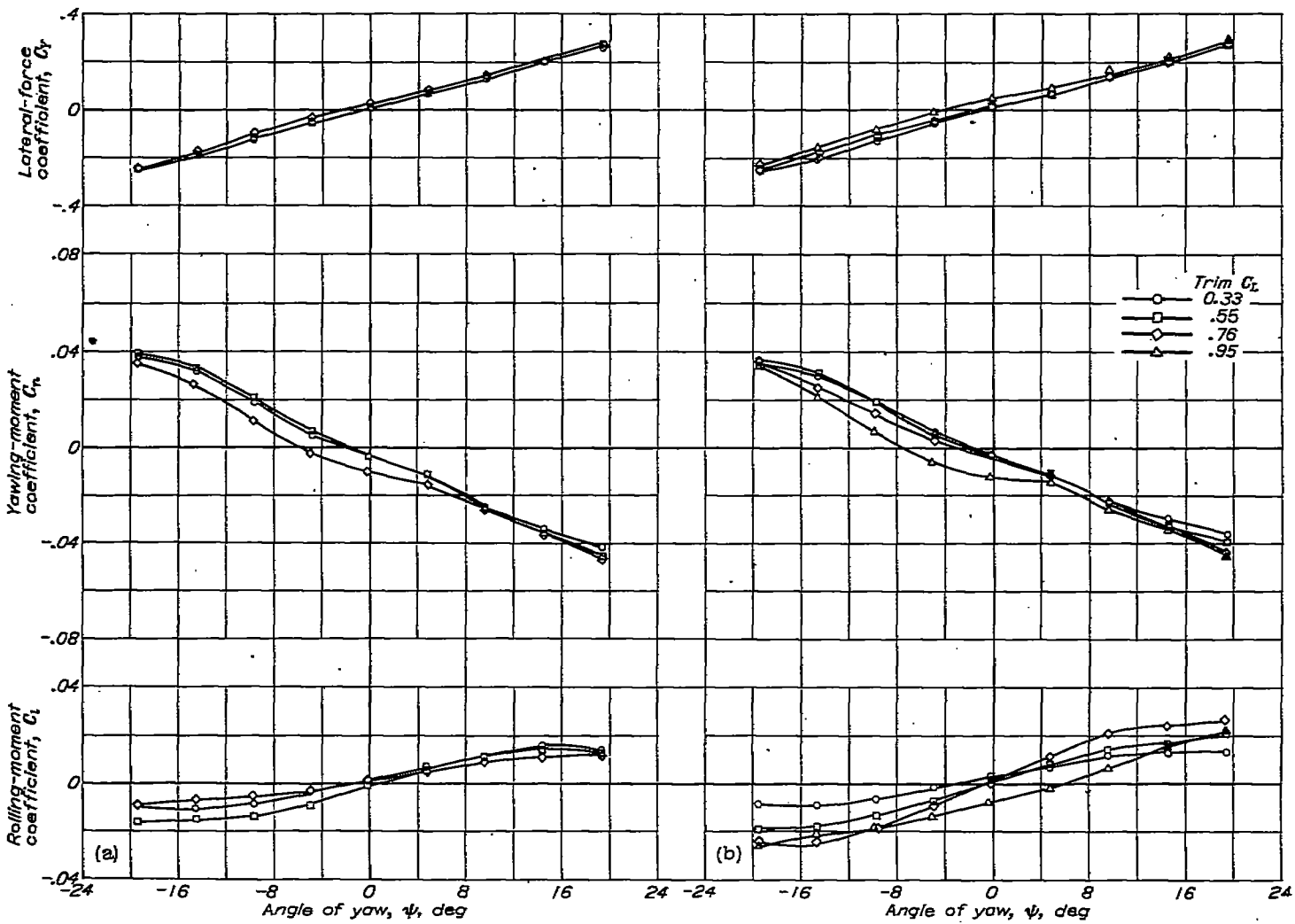

(a) 0-percent-span slots; δ_f=0°.

(b) 0-percent-span slots; δ_f=40°.

FIGURE 11.—Variation of C_Y, C_n, and C_l with angle of yaw. Large ventral fin on; propeller on; R=1.01×10⁶.

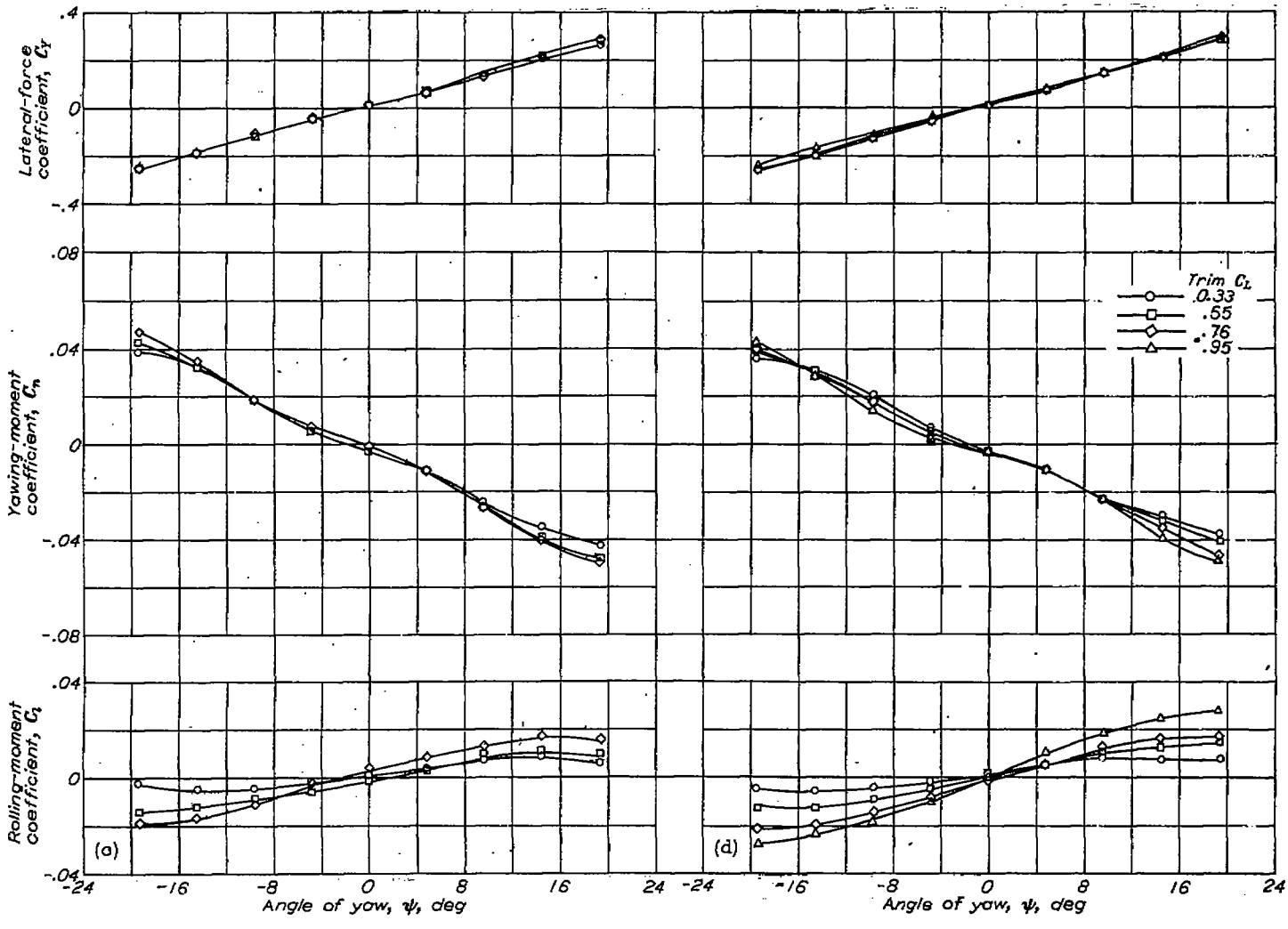

(c) 40-percent-span slots; δ_f=0°.

(d) 40-percent-span slots; δ_f=40°.

FIGURE 11.—Continued.

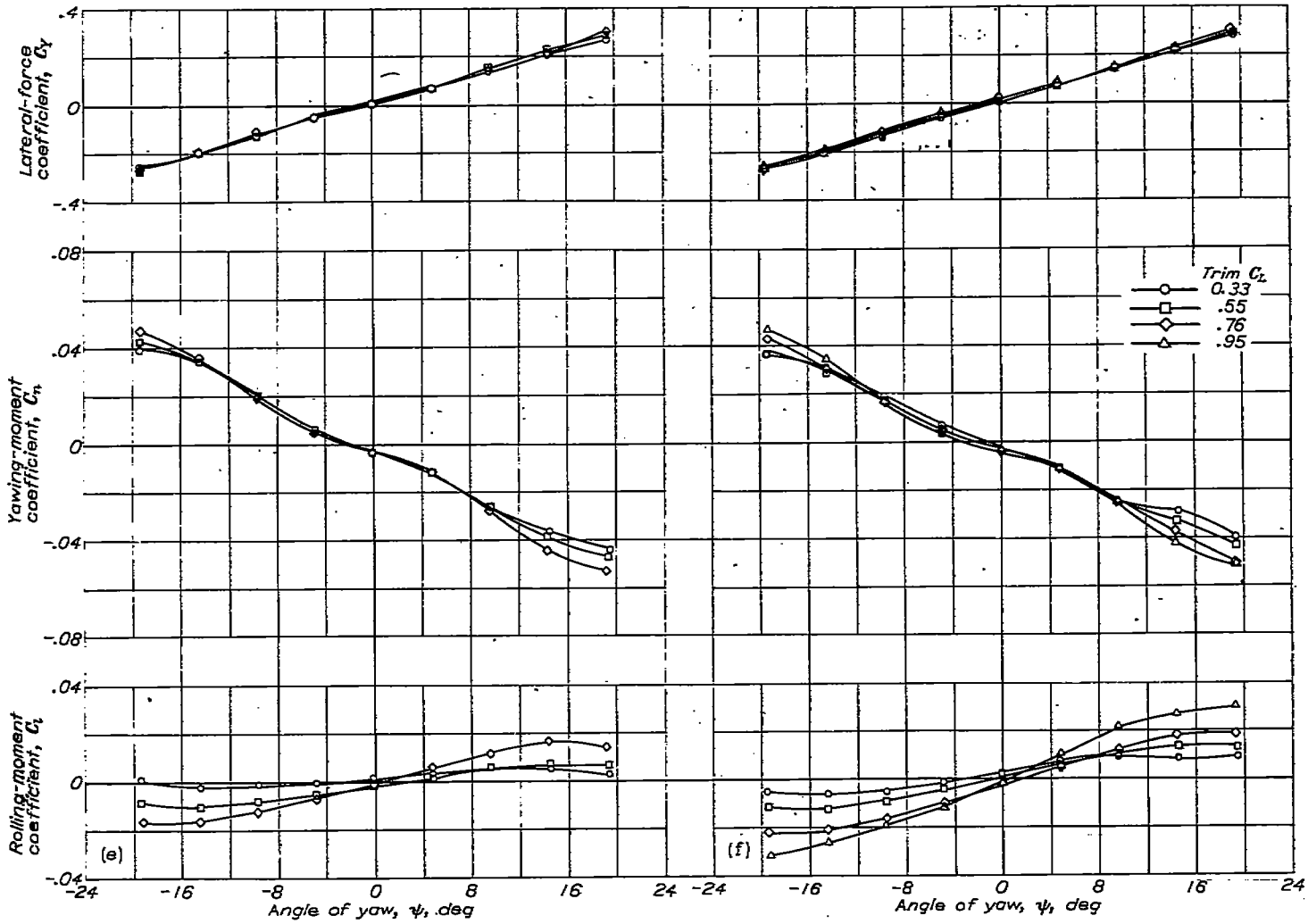

(e) 80-percent-span slots; δ_f=0°

(f) 80-percent-span slots; δ_f=40°

FIGURE 11.—Continued.

RUDDER KICKS

Rudder kicks were initiated by abruptly deflecting the rudder of the airplane and holding this deflection as the airplane responded. The records of the flight motions were short, usually covering 5 seconds. As in the case of the lateral oscillations discussed previously, some slight aileron waggle that occurred was accounted for in the calculated motions. The agreement between the flight and calculated motions is, in general, quite good (figs. 25 to 31). Agreement is best at the lower lift coefficients; however at a lift coefficient of 0.919 (fig. 28), good agreement is shown between flight and calculated angles of sideslip and rolling velocities.

The flight tests reported in reference 5 showed that at low lift coefficients the airplane rolled in response to a rudder kick as if the airplane had a decided negative dihedral effect. Figure 31 indicates that this peculiar response was largely caused by the slight aileron waggle which occurred during the motion. In general, for all configurations investigated, it was found necessary to account for any slight aileron movements in order to predict satisfactorily the lateral motions of the airplane.

The motions at C_L=0.794 (fig. 30) give evidence of departure of the experimental derivatives from the true variation with lift coefficient. This result again is the Reynolds number effect previously discussed. The flight and calculated periods of the lateral oscillation caused by the rudder kicks are in very good agreement which indicates again that the values of C_{n_β} used in the calculations were reasonably accurate.

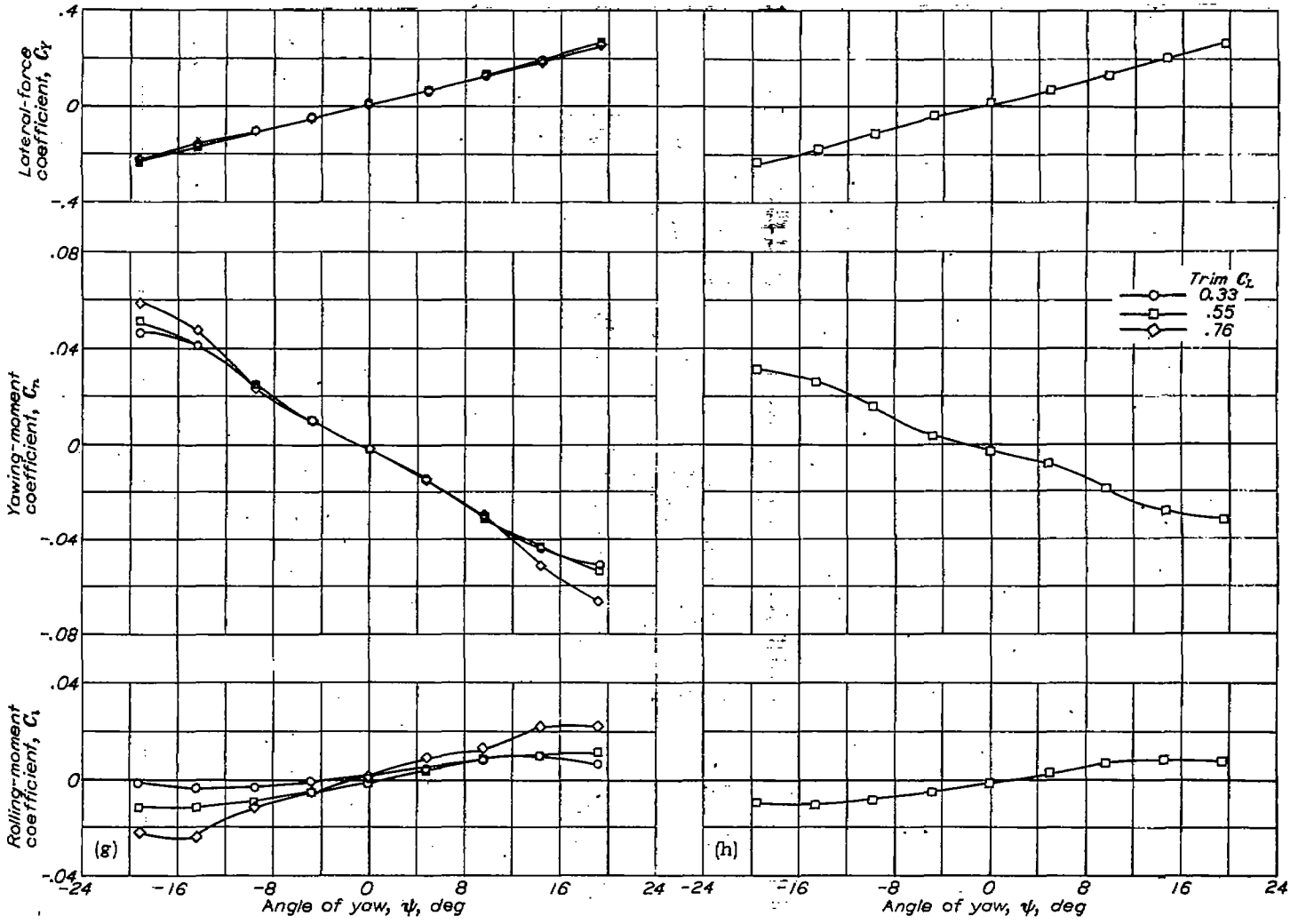

(g) 40-percent-span slots; δ_f=0°; propeller off.

(h) 80-percent-span slots; δ_f=0°; small ventral fin on.

FIGURE 11.—Concluded.

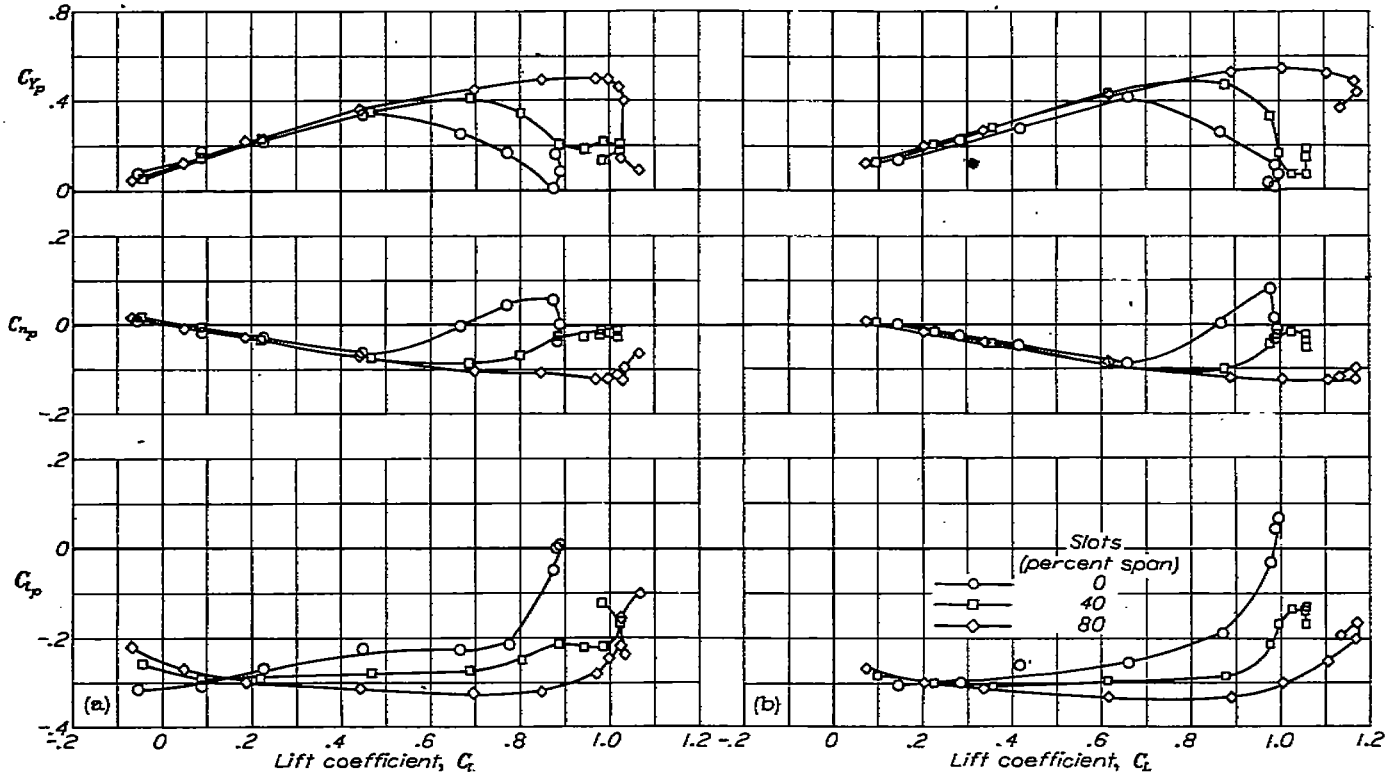

(a) Trim C_L=0.33; δ_f=0°. (b) Trim C_L=0.76; δ_f=40°.

FIGURE 12.—Variation of rolling-stability derivatives with lift coefficient for three slot configurations. ψ=0°; R=1.01×10⁶.

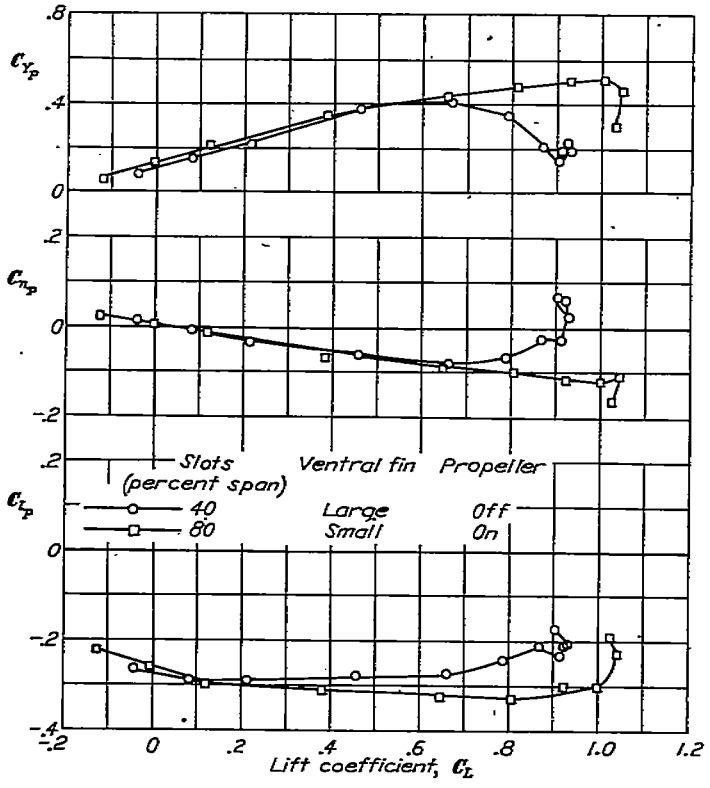

FIGURE 13.—Variation of rolling-stability derivatives with lift coefficient for two slot configurations. ψ=0°; δ_f=0°; R=1.01×10⁶.

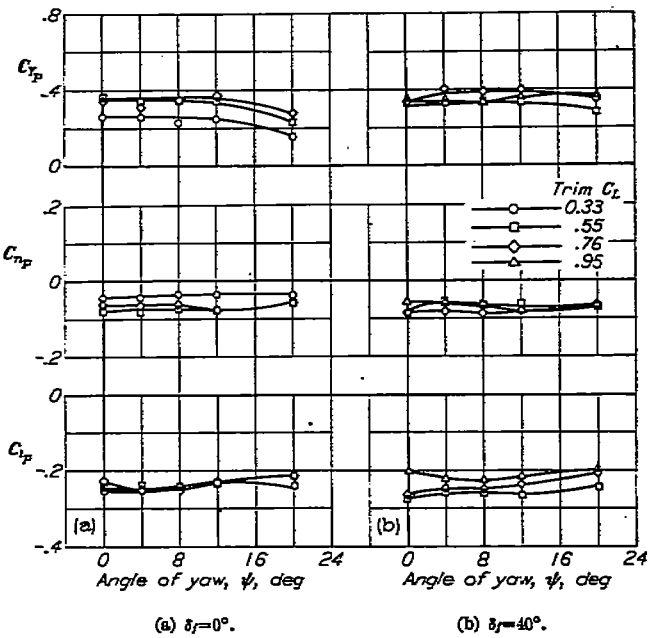

(a) δ_f=0°. (b) δ_f=40°.

FIGURE 14.—Variation of rolling-stability derivatives with angle of yaw. Large ventral fin on; propeller on; 40-percent-span slots; R=1.01×10⁶.

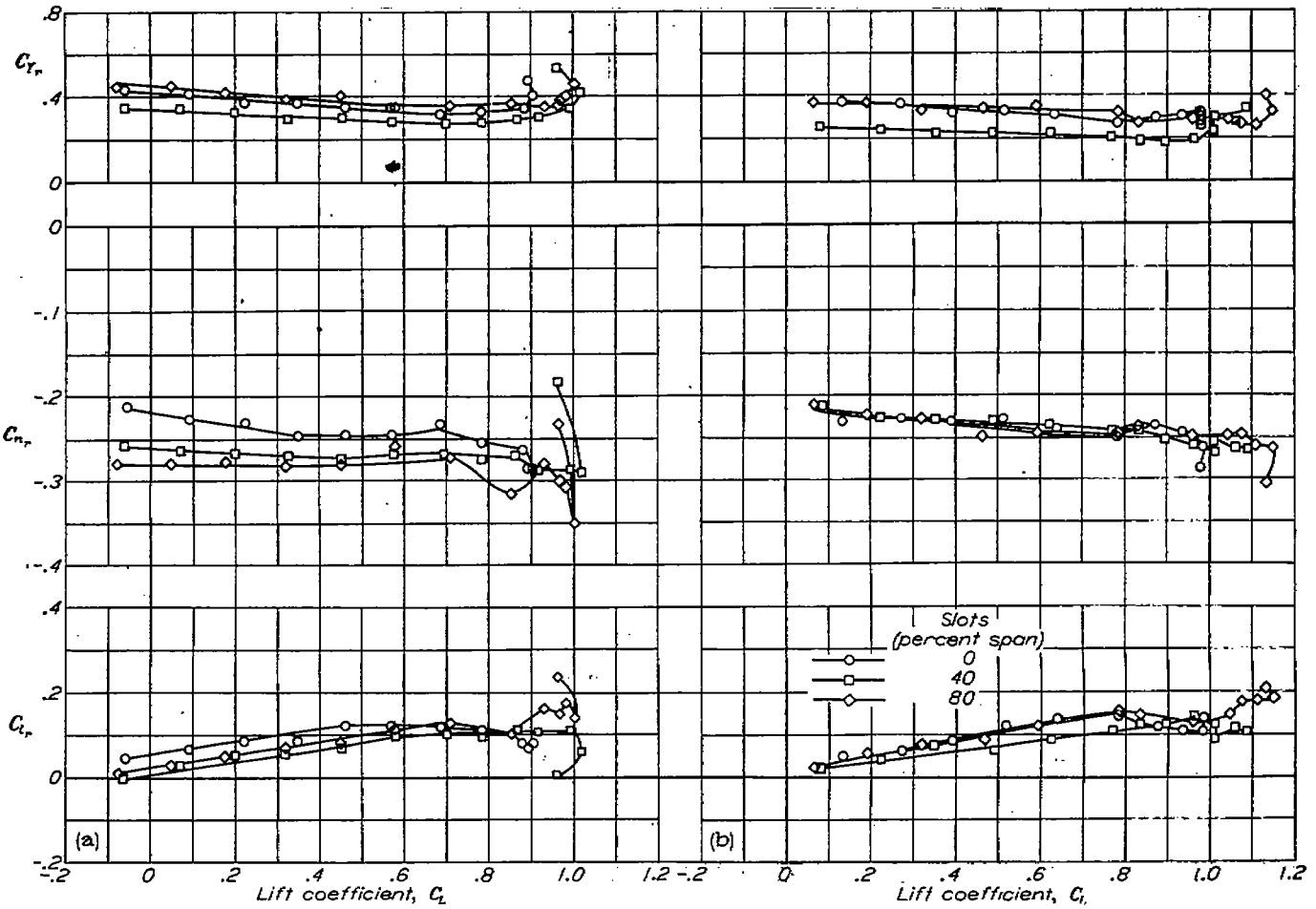

(a) Trim C_L=0.33; δ_f=0°. (b) Trim C_L=0.76; δ_f=40°.

FIGURE 15.—Variation of yawing-stability derivatives with lift coefficient for three slot configurations. Large ventral fin on; propeller on; ψ=0°; R=0.8×10⁶.

AILERON ROLLS

Aileron rolls were initiated by abruptly deflecting the aileron control of the airplane and holding the deflected position as the airplane responded. The rudder control was held as near neutral as possible. The records of motion were necessarily short because of the large angles of bank assumed by the airplane after a short period of time.

Comparison of the flight and calculated aileron rolls indicates fairly good agreement (figs. 32 to 35) except for the high-lift-coefficient condition without nose slots. The stability derivatives for the unslotted configuration show a departure at fairly low lift coefficient from the initial trend of the variation of the derivatives with lift coefficient. As previously mentioned, this result is not obtained at the flight Reynolds numbers. The calculations for this high lift coefficient were carried out with two sets of stability derivatives. One set was obtained by a linear extrapolation of the curves of the derivatives plotted against lift coefficient and the second set, by selecting for the value of the derivative that value just previous to the final break in the curves of the derivatives plotted against lift coefficient. The second procedure was necessary because the flight lift coefficient was greater than the maximum experimental lift coefficient. The linear extrapolation produces the better result, but it can be seen that neither set of derivatives was very satisfactory although it would appear logical to believe, in view of the Reynolds number effects indicated previously, that the linear extrapolation of the derivatives would have given fairly good results. The aileron roll for the 80-percent-span slot configuration with flaps down at C_L=1.169 (fig. 35) shows fair agreement between the flight and calculated motions so that a beneficial effect of the slots in maintaining an unseparated

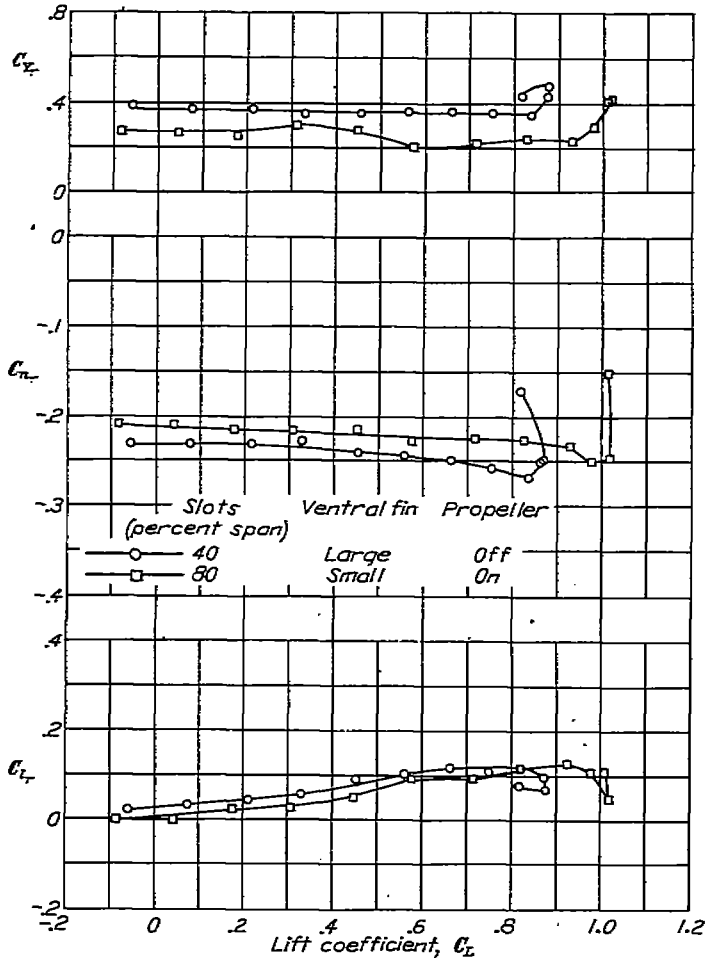

FIGURE 16.—Variation of yawing-stability derivatives with lift coefficient for two slot configurations. Trim C_L=0.33; ψ=0°; δ_r=0°; R=0.8×10⁶.

flow over the wing to a fairly high lift coefficient is indicated.

The effects of elasticity of the wing were not considered in the calculations of the aileron rolls because of lack of knowledge of the flexibility of the wing. Rough estimates of the effect of elasticity on the rolling velocity for the results of figure 33 indicate that the discrepancies shown between flight and calculated results would be reduced by about 50 percent or more.

A comparison has been made of the maximum rolling velocities obtained by calculation for conditions duplicating those in flight, by flight tests, and by calculations for a coordinated maneuver in which the yawing velocity and angle of sideslip are maintained at zero. For this last case, the rolling velocity becomes

$$p=\frac{-\Delta C_l}{C_{l_p}}\frac{2V}{b}$$

The results are presented in the following table:

Figure	Maximum rolling velocities from figures			$\left\lvert\frac{\Delta C_l}{C_{l_p}}\right\rvert\frac{2V}{b}$
	Calculated	Flight (left)	Flight (right)	
32	0.62	0.44	----	2.67
33	.77	.60	0.53	1.11
34	.78	----	.67	1.13
35	.34	.33	.30	.68

The comparison indicates that a marked difference may be obtained in the maximum rolling velocity by eliminating the degrees of freedom of sideslip and yaw. This last method of calculation is used frequently in comparing the relative merits of various forms of ailerons.

NONLINEAR CALCULATIONS

Calculations, in which the curves of C_l and C_n against ψ were represented not by a single slope but by a series of tangents to the curves and in which the variation of C_{n_r} with ψ was included, were made for two motions to illustrate the effect of these nonlinearities. The results are given in figures 36 and 37 along with the flight motion and the calculations made for linear slopes and constant damping derivatives. The effect of the aileron waggle was small and was taken to be the same as for the linear calculation. These figures indicate that for the angles of sideslip encountered in these motions little is to be gained by going to the additional effort required to make the calculations for the nonlinear case. The nonlinear calculations required approximately ten times as long to complete as the linear calculations. Motions at large angles of sideslip or motions for a configuration having more pronounced nonlinearities than for the airplane considered herein would undoubtedly show the nonlinearities to be of greater significance.

SUMMARY OF RESULTS

The investigation indicated that the lateral disturbed motions of the airplane considered herein may be generally calculated with good accuracy by the use of experimental-scale-model data up to lift coefficients where any appreciable effects of the difference in Reynolds number between the scale and flight conditions begin to be apparent. This effect is usually evidenced by a departure of the scale results from a gradual variation with lift coefficient and, for the case investigated, corresponds to a lift coefficient of 0.8 for the slotted-wing configurations. At higher lift coefficients the accuracy in calculating flight motions is progressively

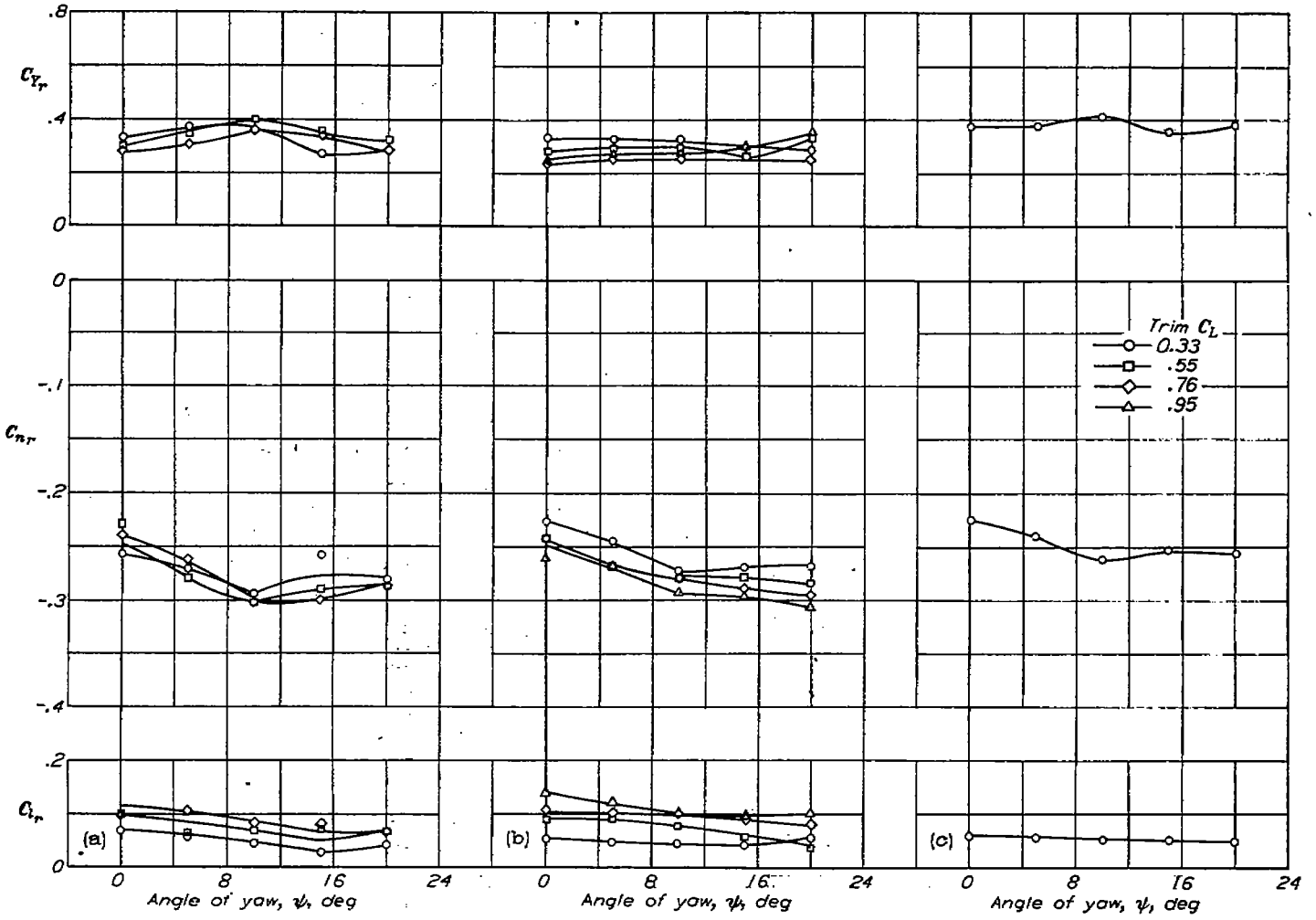

(a) δ_f=0°; propeller on. (b) δ_f=40°; propeller on. (c) δ_f=0°; propeller off.

FIGURE 17.—Variation of yawing-stability derivatives with angle of yaw. Large ventral fin on; 40-percent-span slots; R=0.8×10⁶.

poorer, especially in the time to damp to half amplitude where errors as much as 100 percent or more may be encountered. For the airplane of this investigation, at these high lift coefficients, the calculated time to damp to half amplitude was generally higher than the flight value. In most cases the period of the motion could be calculated to within 5 percent of that obtained in the flight motion. In order to obtain good accuracy in predicting flight motions, proper consideration of all control movements must be made.

For most cases, the nonlinear variation of the directional-stability parameter, the effective dihedral parameter, and the variation of the damping in yaw with angle of yaw could be neglected. If, however, the flight motions reach a sufficiently large amplitude for a long period of time, as in an aileron roll for example, greater accuracy in the calculated motions should result if the nonlinearities in the variation of yawing-moment coefficient, rolling-moment coefficient, and damping in yaw with angle of yaw are included in the calculations.

LANGLEY AERONAUTICAL LABORATORY,
NATIONAL ADVISORY COMMITTEE FOR AERONAUTICS,
LANGLEY FIELD, VA., *November 1, 1949.*

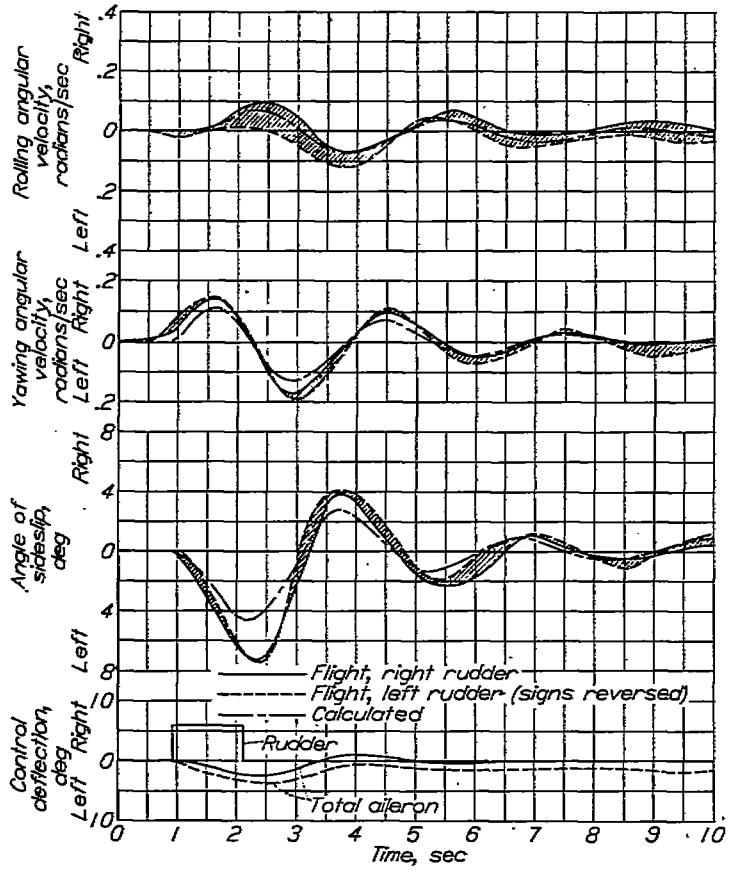

FIGURE 18.—Comparison of the flight and calculated lateral motions resulting from an abrupt deflection and release of the rudder. 40-percent-span slots; flaps up; C_L=0.334; V_C=198 miles per hour; engine idling.

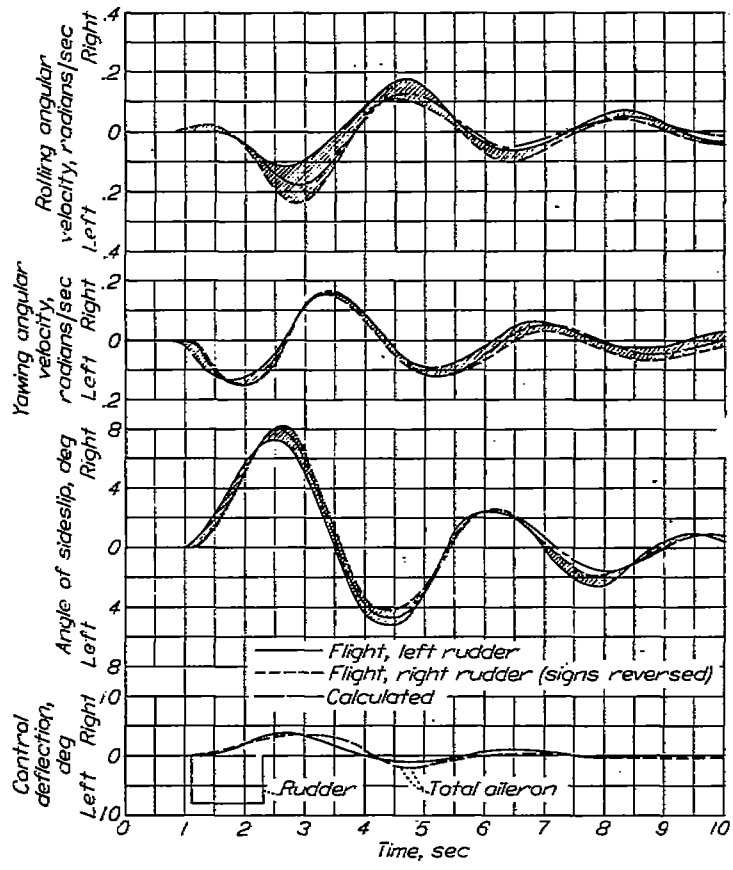

FIGURE 19.—Comparison of flight and calculated lateral motions resulting from an abrupt deflection and release of the rudder. 40-percent-span slots; flaps up; C_L=0.551; V_C=156 miles per hour; engine idling.

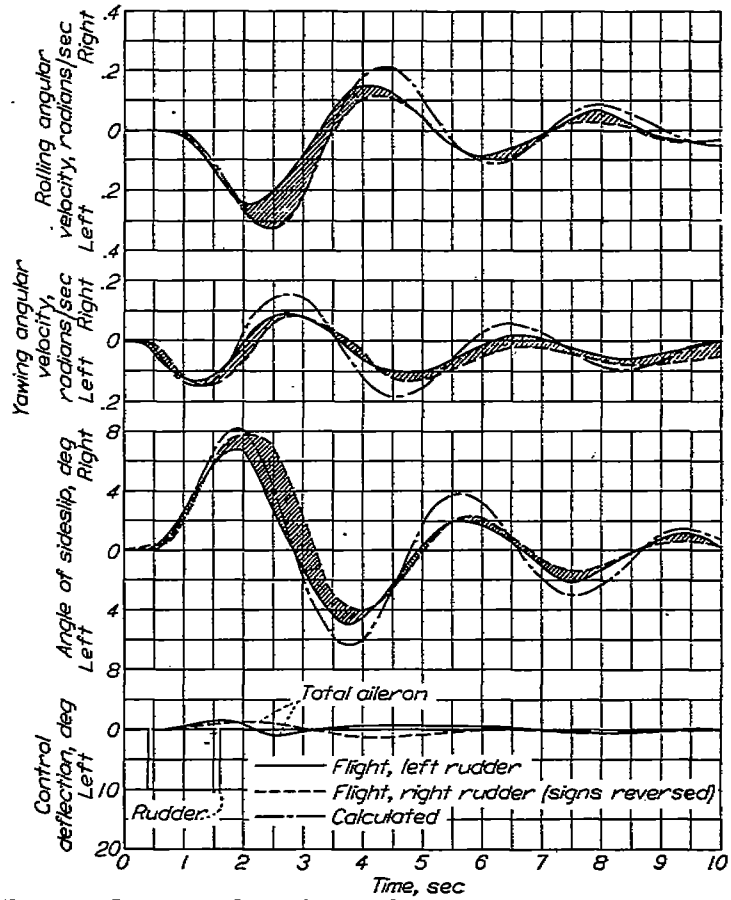

FIGURE 20.—Comparison of flight and calculated lateral motions resulting from an abrupt deflection and release of the rudder. 40-percent-span slots; flaps up; C_L=0.759; V_C=136 miles per hour; engine idling.

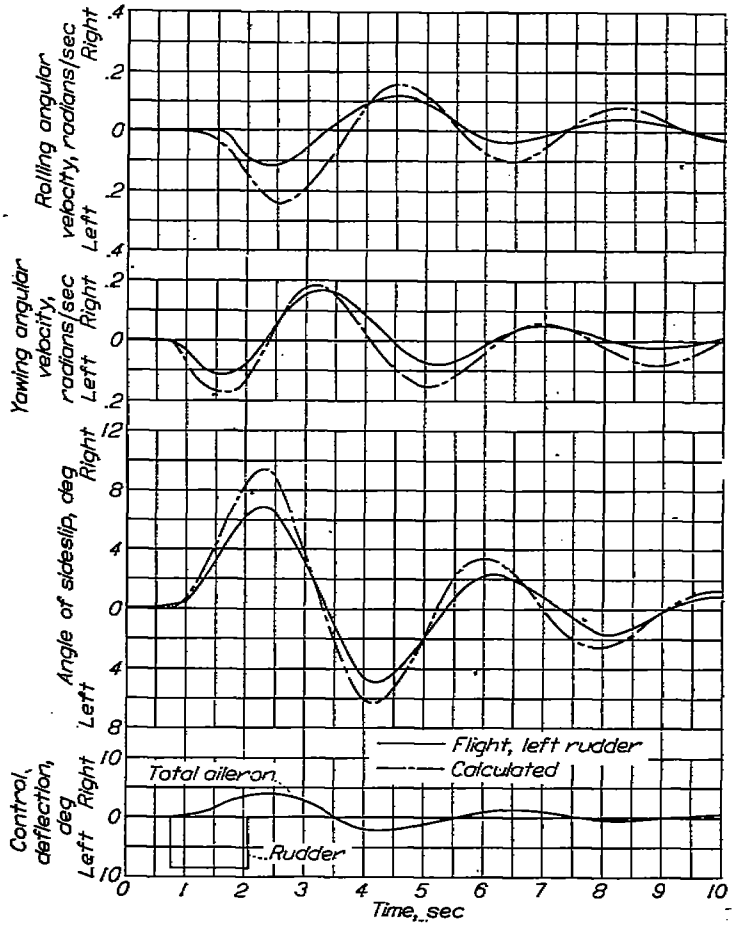

FIGURE 21.—Comparison of flight and calculated lateral motions resulting from an abrupt deflection and release of the rudder. 40-percent-span slots; flaps down; C_L=0.524; V_C=160 miles per hour; engine idling.

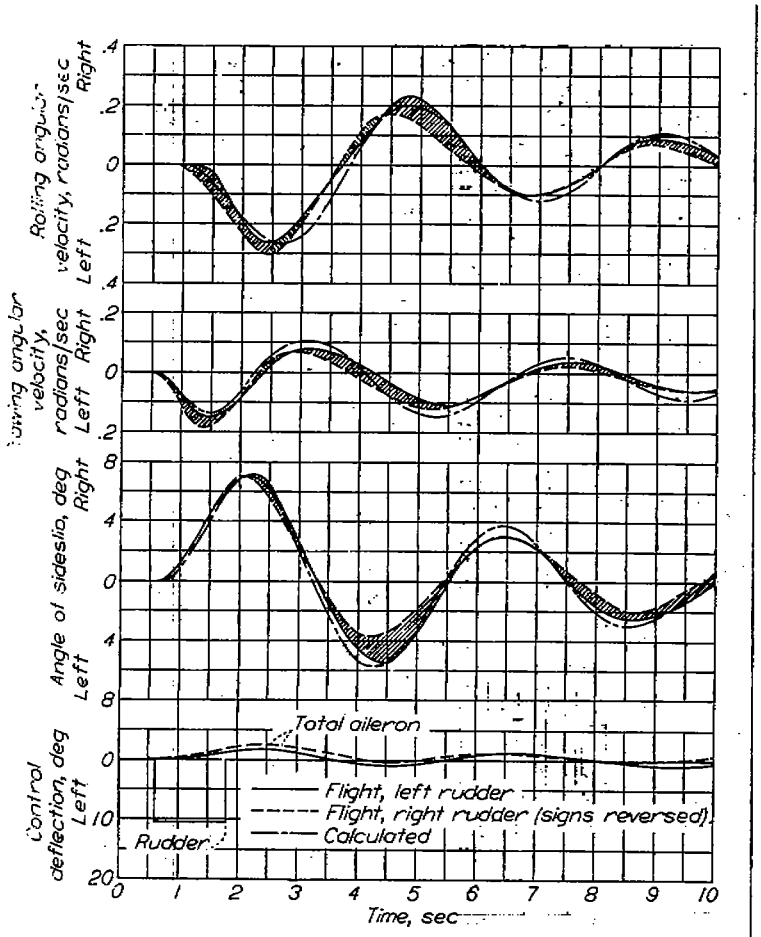

FIGURE 22.—Comparison of flight and calculated lateral motions resulting from an abrupt deflection and release of the rudder. 40-percent-span slots; flaps down; C_L=0.801; V_C=128 miles per hour; engine idling.

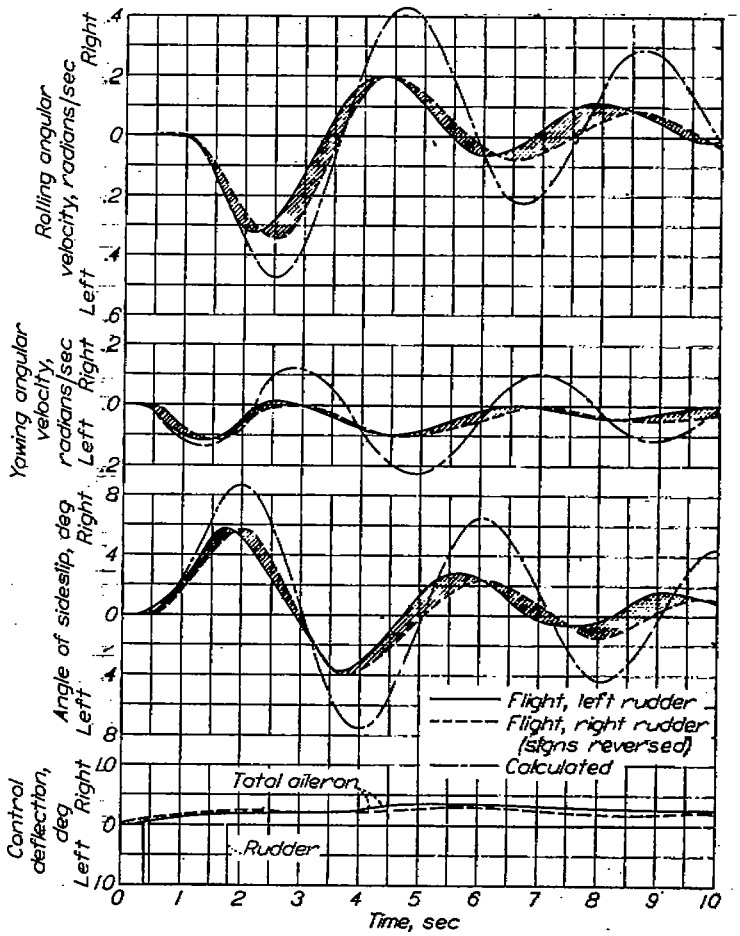

FIGURE 23.—Comparison of flight and calculated lateral motions resulting from an abrupt deflection and release of the rudder. 80-percent-span slots; flaps up; small ventral fin on; C_L=0.977; V_C=120 miles per hour; engine idling.

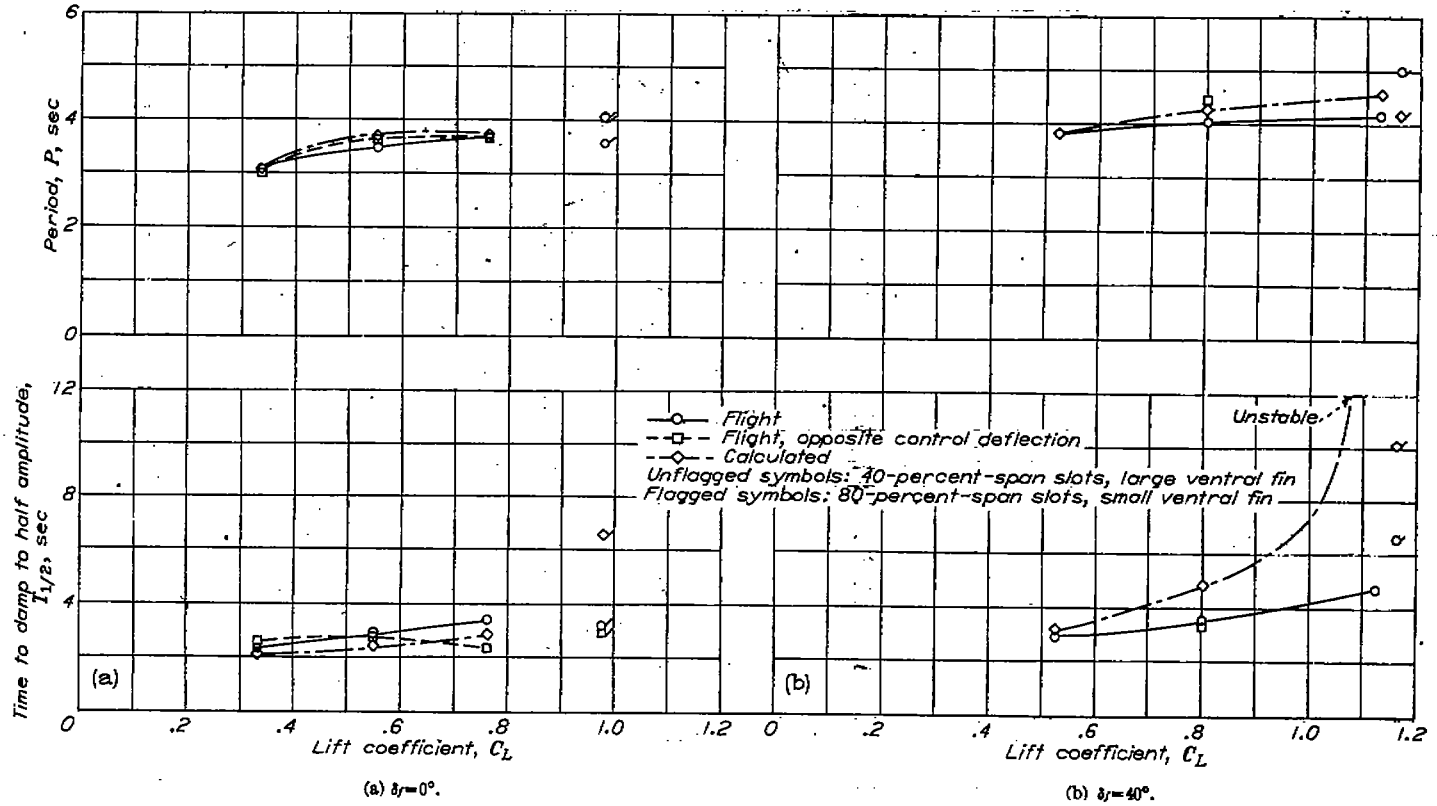

(a) δ_f=0°. (b) δ_f=40°.

FIGURE 24.—Comparison of flight and calculated values of the period and time to damp to half amplitude.

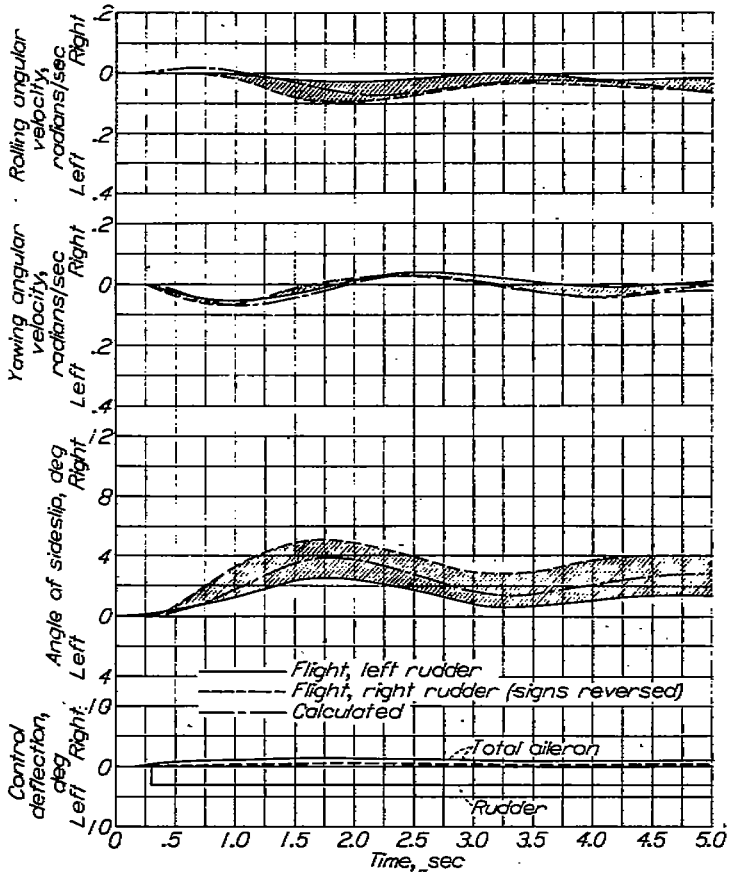

FIGURE 25.—Comparison of flight and calculated lateral motions resulting from a left rudder kick. 40-percent-span slots; flaps up; C_L=0.341; V_c=198 miles per hour; engine idling.

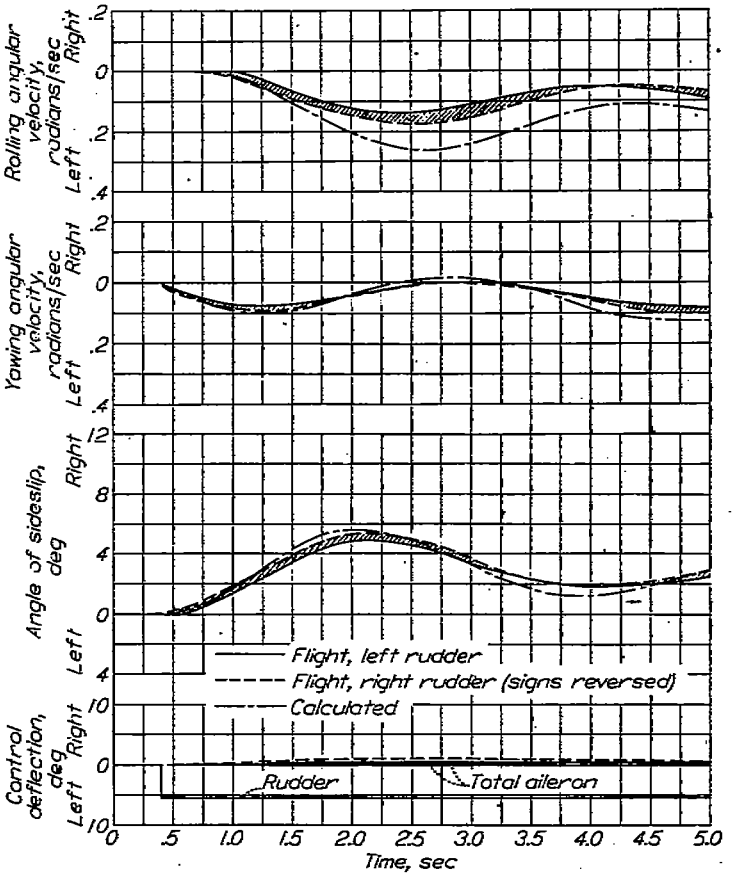

FIGURE 26.—Comparison of flight and calculated lateral motions resulting from a left rudder kick. 40-percent-span slots; flaps up; C_L=0.556; V_c=160 miles per hour; engine idling.

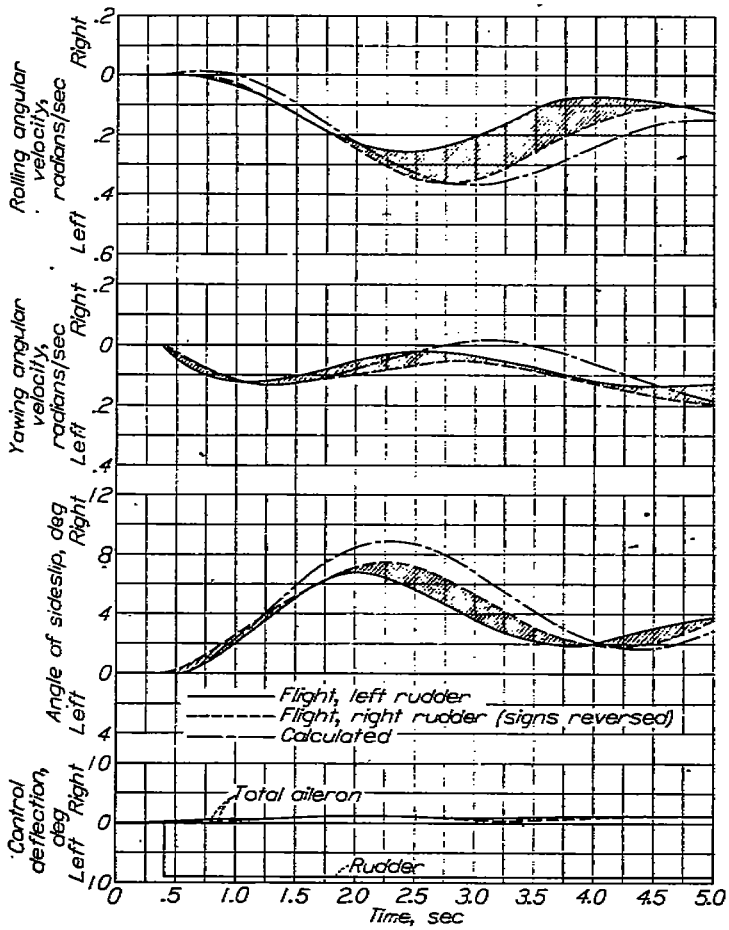

FIGURE 27.—Comparison of flight and calculated lateral motions resulting from a left rudder kick. 40-percent-span slots; flaps up; C_L=0.764; V_c=133 miles per hour; engine idling.

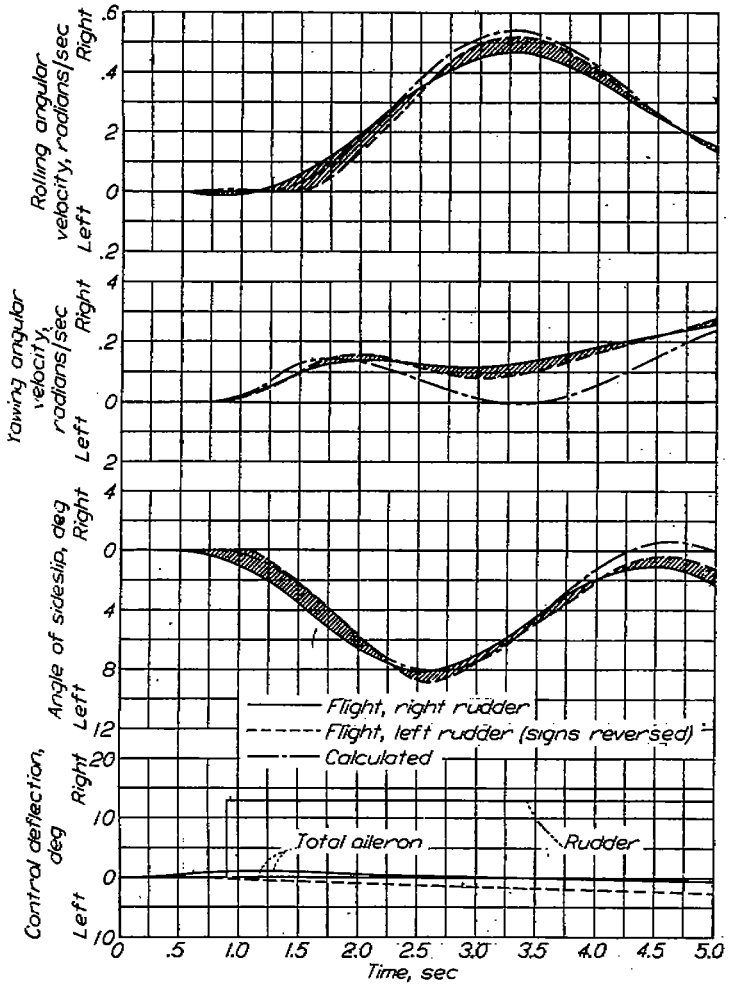

FIGURE 28.—Comparison of flight and calculated lateral motions resulting from a right rudder kick. 40-percent-span slots; flaps up; C_L=0.919; V_C=120 miles per hour; engine idling.

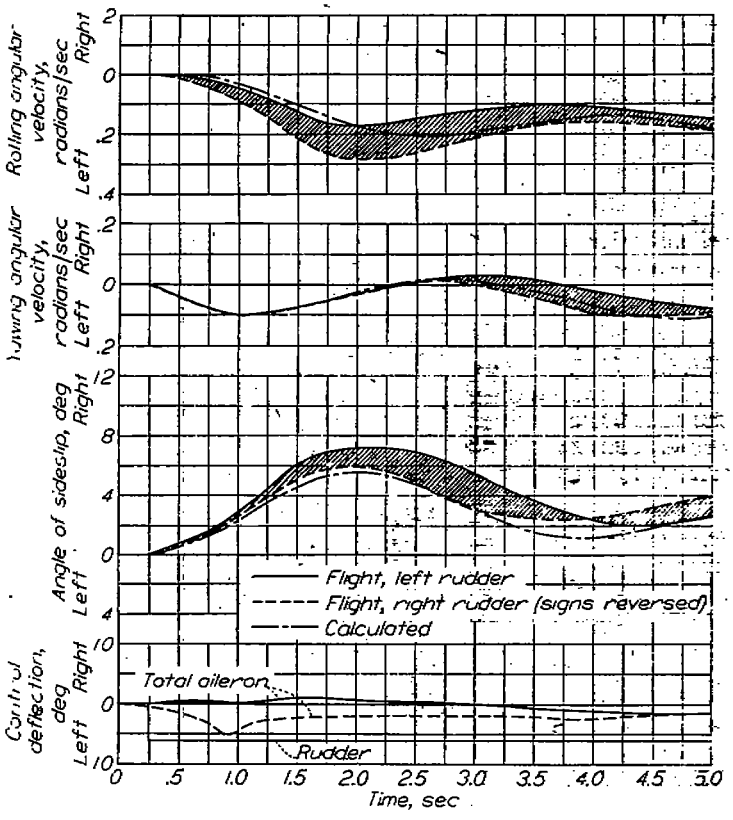

FIGURE 29.—Comparison of flight and calculated lateral motions resulting from a left rudder kick. 40-percent-span slots; flaps down; C_L=0.537; V_C=157 miles per hour; engine idling.

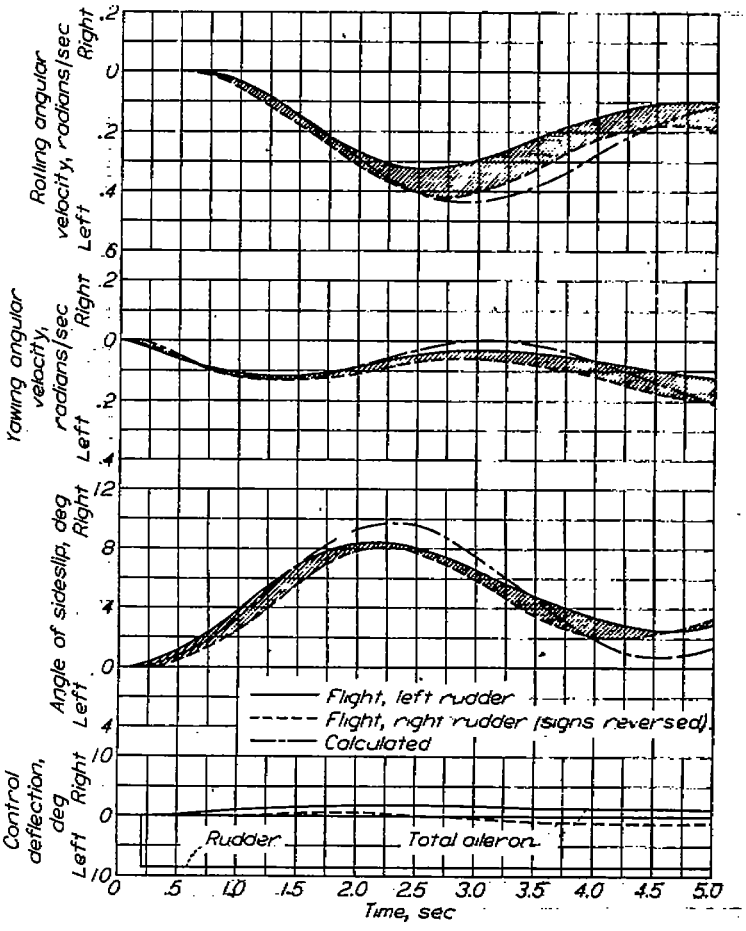

FIGURE 30.—Comparison of flight and calculated lateral motions resulting from a left rudder kick. 40-percent-span slots; flaps down; C_L=0.794; V_C=130 miles per hour; engine idling.

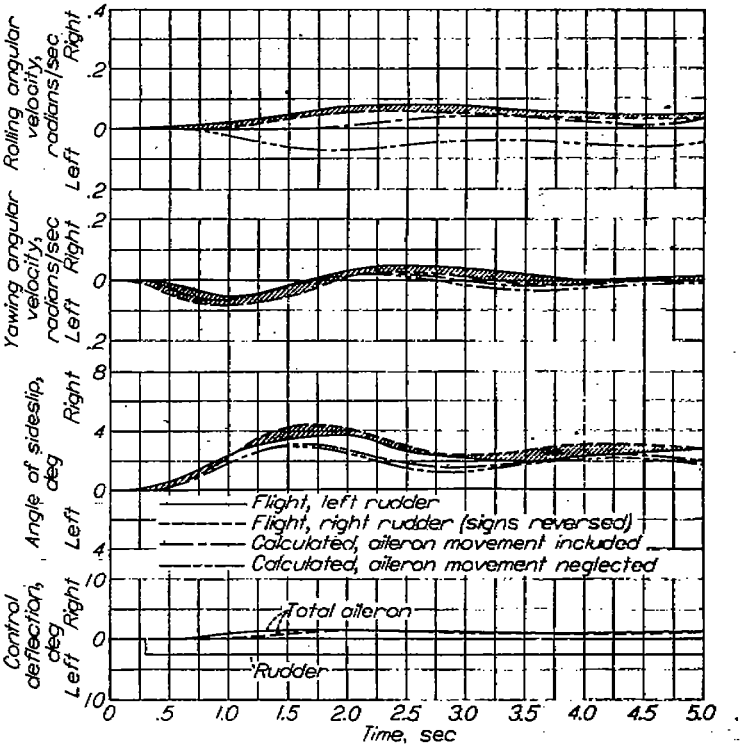

FIGURE 31.—Comparison of flight and calculated lateral motions resulting from a left rudder kick. 80-percent-span slots; flaps up; C_L=0.278; V_C=228 miles per hour; engine idling.

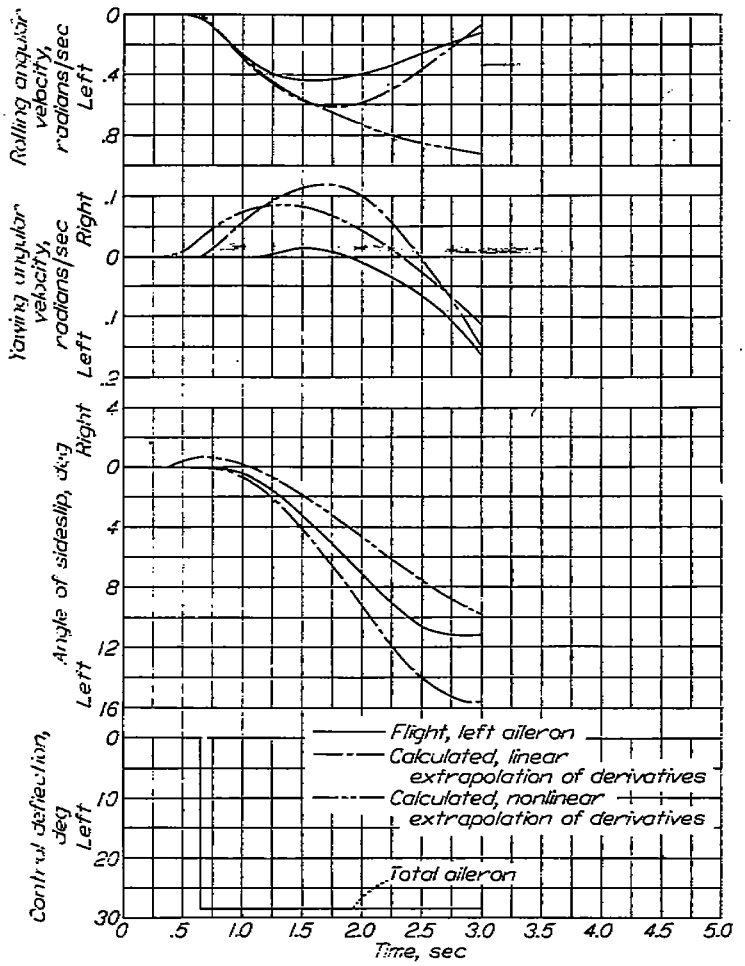

FIGURE 32.—Comparison of flight and calculated lateral motions resulting from an abrupt left aileron deflection. 0-percent-span slots; flaps up; C_L=0.983; V_C=119 miles per hour; engine idling.

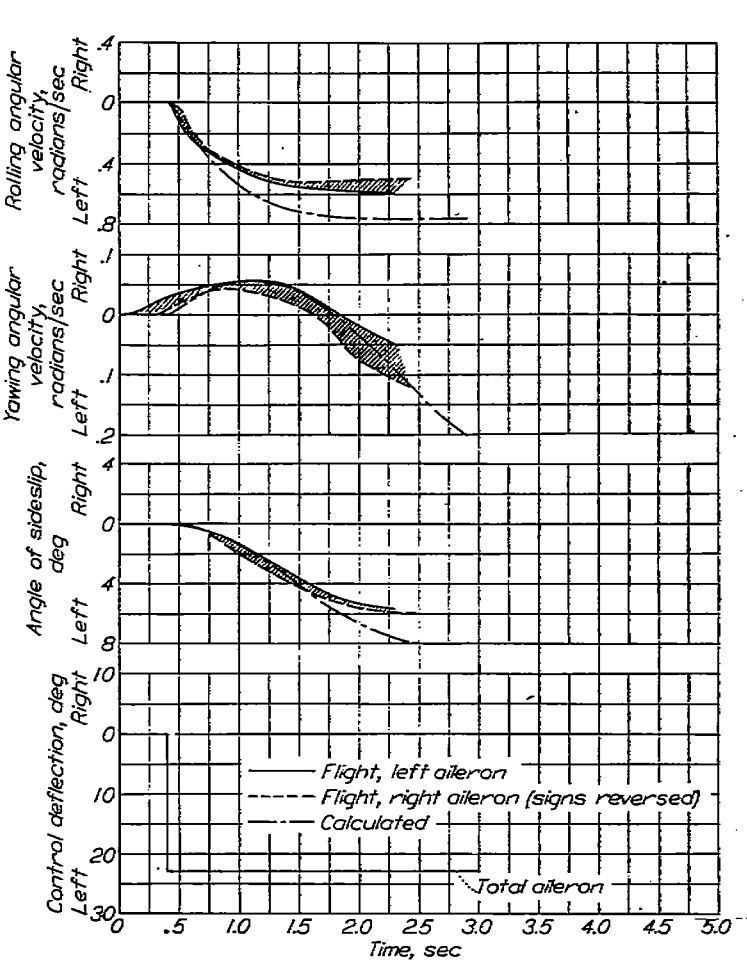

FIGURE 33.—Comparison of flight and calculated lateral motions resulting from an abrupt left aileron deflection. 40-percent-span slots; flaps up; C_L=0.598; V_C=150 miles per hour; engine idling.

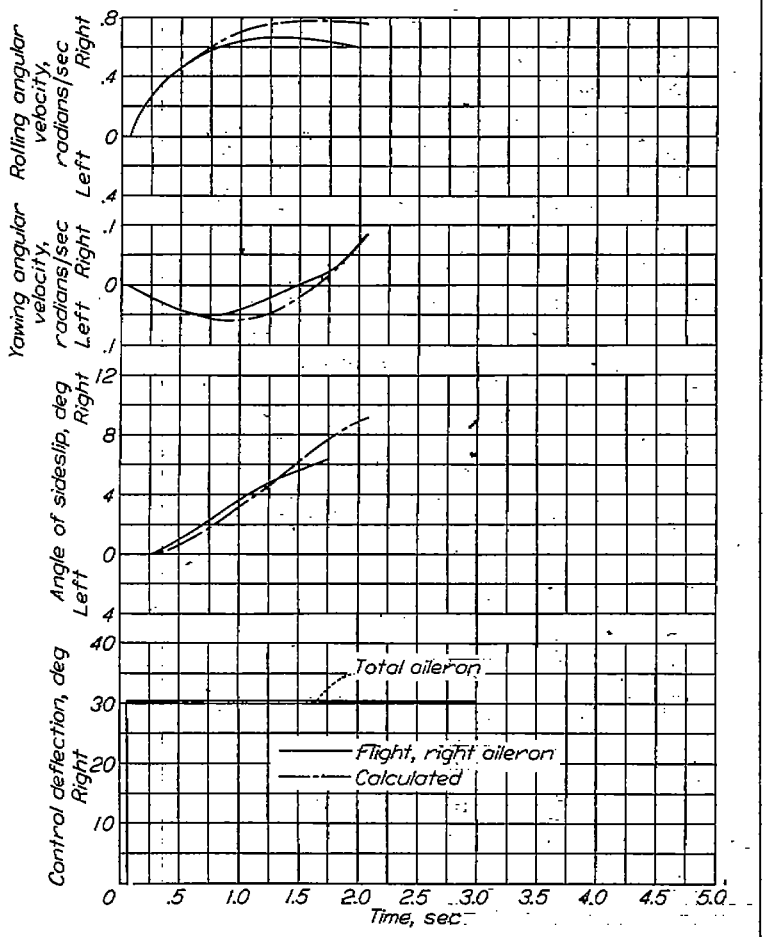

FIGURE 34.—Comparison of flight and calculated lateral motions resulting from an abrupt right aileron deflection. 40-percent-span slots; flaps down; C_L=0.598; V_C=146 miles per hour; engine idling.

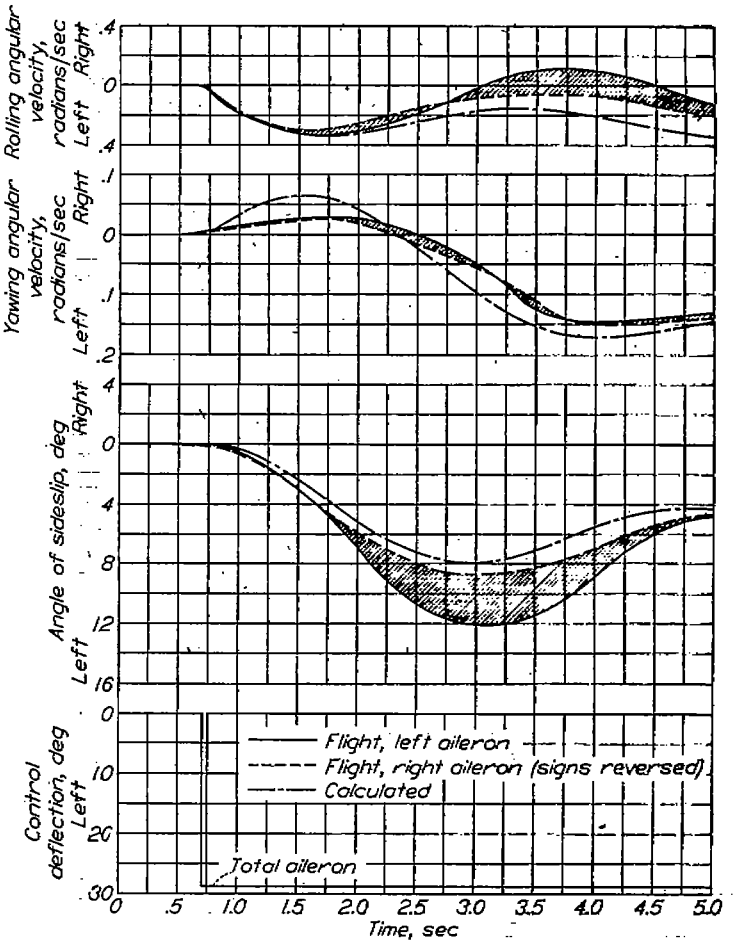

FIGURE 35.—Comparison of flight and calculated lateral motions resulting from an abrupt left aileron deflection. 80-percent-span slots; flaps down; C_L=1.169; V_C=110 miles per hour; engine idling.

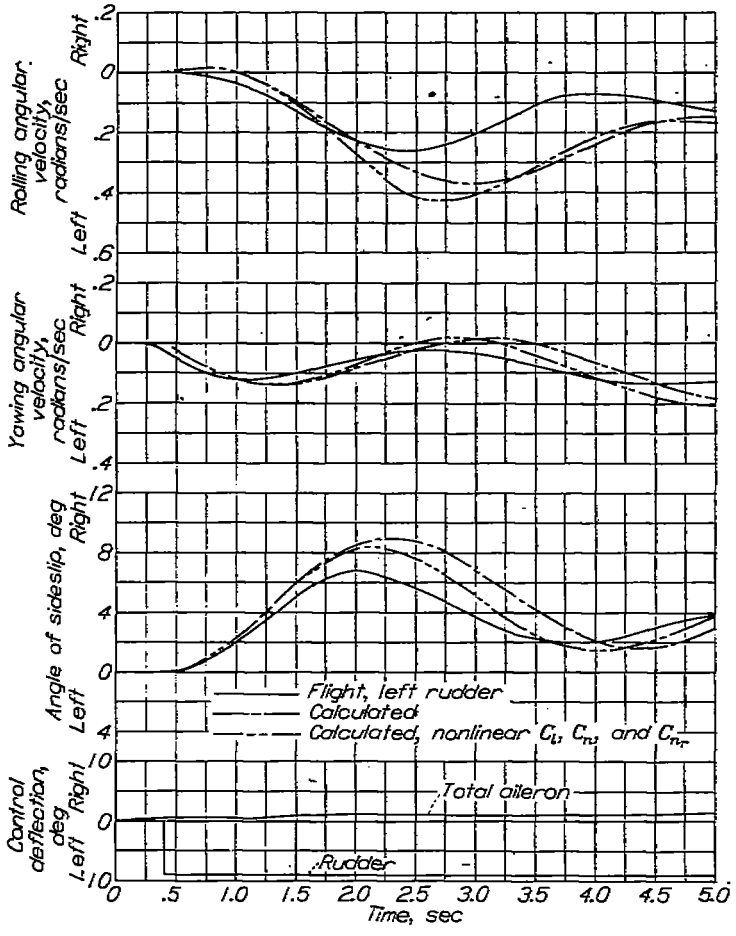

FIGURE 36.—Effect of nonlinear variation of C_l, C_n, and C_{n_r} with angle of yaw on the calculated lateral motions resulting from a left rudder kick. 40-percent-span slots; flaps up; C_L=0.764; V_C=133 miles per hour; engine idling.

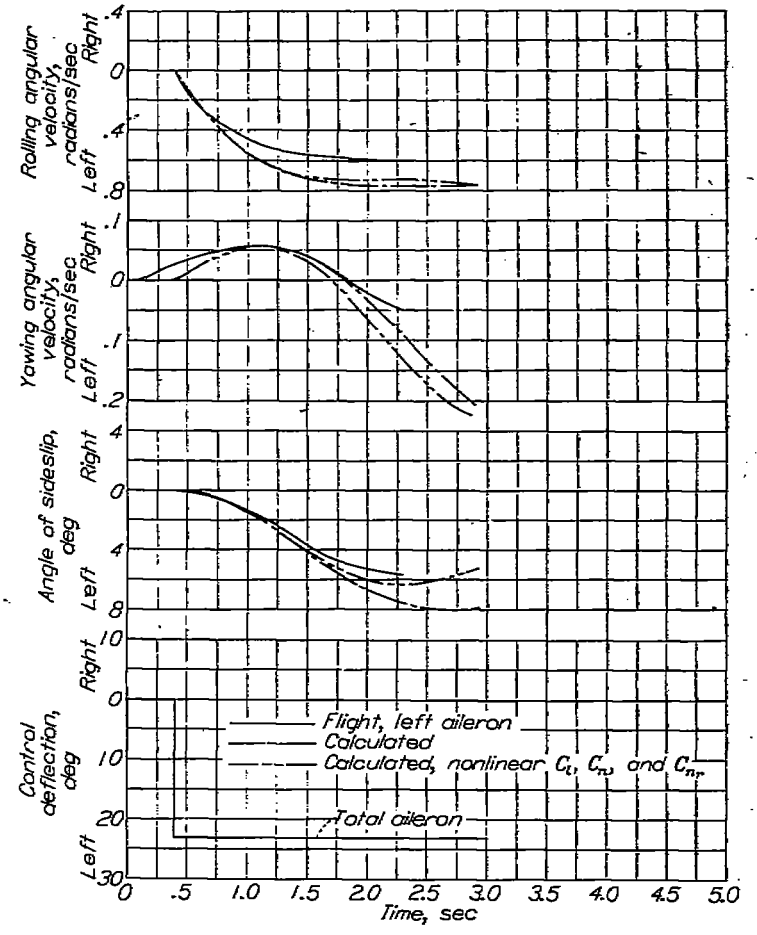

FIGURE 37.—Effect of nonlinear variation of C_l, C_n, and C_{n_r} with angle of yaw on the calculated lateral motions resulting from an abrupt left aileron deflection. 40-percent-span slots; flaps up, C_L=0.598; V_C=150 miles per hour; engine idling.

APPENDIX

LATERAL EQUATIONS OF MOTION

The lateral equations of motions used for most of the calculations of this report consider the fluctuation of the aerodynamic forces to be directly proportional to the component angular and translational velocities associated with the axis system as is customary in classical stability theory. The modification to these equations to account for the nonlinear effects of sideslip is discussed in the text. The equations used herein contain the necessary product of inertia and control terms and are given as follows:

Roll

$$C_{l_{\delta_r}}\delta_r+C_{l_{\delta_a}}\delta_a+C_{l_\beta}\beta+\frac{1}{2}C_{l_p}D\varphi+\frac{1}{2}C_{l_r}D\psi=2\mu\left\{\left[\left(\frac{k_{X_0}}{b}\right)^2\cos^2\eta+\left(\frac{k_{Z_0}}{b}\right)^2\sin^2\eta\right]D^2\varphi+\left[\left(\frac{k_{Z_0}}{b}\right)^2-\left(\frac{k_{X_0}}{b}\right)^2\right]\cos\eta\sin\eta\,D^2\psi\right\}$$

Yaw

$$C_{n_{\delta_r}}\delta_r+C_{n_{\delta_a}}\delta_a+C_{n_\beta}\beta+\frac{1}{2}C_{n_p}D\varphi+\frac{1}{2}C_{n_r}D\psi=2\mu\left\{\left[\left(\frac{k_{Z_0}}{b}\right)^2\cos^2\eta+\left(\frac{k_{X_0}}{b}\right)^2\sin^2\eta\right]D^2\psi+\left[\left(\frac{k_{Z_0}}{b}\right)^2-\left(\frac{k_{X_0}}{b}\right)^2\right]\cos\eta\sin\eta\,D^2\psi\right\}$$

Sideslip

$$C_{Y_{\delta_r}}\delta_r+C_{Y_{\delta_a}}\delta_a+C_{Y_\beta}\beta+\frac{1}{2}C_{Y_p}D\varphi+\frac{1}{2}C_{Y_r}D\psi+C_L\varphi+C_L\psi\tan\gamma=2\mu(D\beta+D\psi)$$

where

$D=\frac{d}{ds}$

$s=\frac{TV}{b}$

$C_{l_{\delta_r}}$ rate of change of rolling-moment coefficient with rudder deflection

$C_{l_{\delta_a}}$ rate of change of rolling-moment coefficient with aileron deflection

$C_{n_{\delta_r}}$ rate of change of yawing-moment coefficient with rudder deflection

$C_{n_{\delta_a}}$ rate of change of yawing-moment coefficient with aileron deflection

$C_{Y_{\delta_r}}$ rate of change of lateral-force coefficient with rudder deflection

$C_{Y_{\delta_a}}$ rate of change of lateral-force coefficient with aileron deflection

φ angle of bank, radians

$\mu=\frac{W}{\rho S b g}$

W weight of airplane

g acceleration due to gravity

k_{X_0} radius of gyration about principal longitudinal axis $\left(\sqrt{\frac{I_{X_0}g}{W}}\right)$

k_{Z_0} radius of gyration about principal normal axis $\left(\sqrt{\frac{I_{Z_0}g}{W}}\right)$

γ flight path angle, positive for climb

η inclination of principal longitudinal axis of inertia with respect to flight path, positive when above flight path at nose

$C_{Y_\beta}=\frac{\partial C_Y}{\partial\beta}$

REFERENCES

1. MacLachlan, Robert, and Letko, William: Correlation of Two Experimental Methods of Determining the Rolling Characteristics of Unswept Wings. NACA TN 1309, 1947.
2. Queijo, M. J., and Jaquet, Byron M.: Calculated Effects of Geometric Dihedral on the Low-Speed Rolling Derivatives of Swept Wings. NACA TN 1732, 1948.
3. Goodman, Alex, and Brewer, Jack D.: Investigation at Low Speeds of the Effect of Aspect Ratio and Sweep on Static and Yawing Stability Derivatives of Untapered Wings. NACA TN 1669, 1948.
4. Toll, Thomas A., and Queijo, M. J.: Approximate Relations and Charts for Low-Speed Stability Derivatives of Swept Wings. NACA TN 1581, 1948.
5. Sjoberg, S. A., and Reeder, J. P.: Flight Measurements of the Stability, Control, and Stalling Characteristics of an Airplane Having a 35° Sweptback Wing without Slots and with 80-Percent-Span Slots and a Comparison with Wind-Tunnel Data. NACA TN 1743, 1948.
6. Sjoberg, S. A., and Reeder, J. P.: Flight Measurements of the Lateral and Directional Stability and Control Characteristics of an Airplane Having a 35° Sweptback Wing with 40-Percent-Span Slots and a Comparison with Wind-Tunnel Data. NACA TN 1511, 1948.
7. Lockwood, Vernard E., and Watson, James M.: Stability and Control Characteristics at Low Speed of an Airplane Model Having a 38.7° Sweptback Wing with Aspect Ratio 4.51, Taper Ratio 0.54, and Conventional Tail Surfaces. NACA TN 1742, 1948.
8. Jones, Robert T.: A Simplified Application of the Method of Operators to the Calculation of Disturbed Motions of an Airplane. NACA Rep. 560, 1936.
9. Levy, H., and Baggott, E. A.: Numerical Studies in Differential Equations. Vol. 1, Watts & Co. (London), 1934.
10. Zimmerman, Charles H.: An Analysis of Lateral Stability in Power-Off Flight with Charts for Use in Design. NACA Rep. 589, 1937.

TABLE I.—PERTINENT AIRPLANE DIMENSIONS AND CHARACTERISTICS

Mass characteristics:	
Normal gross weight, lb	8,700
Moments of inertia, ft-lb-sec²:	
I_{X_0}	7,654
I_{Y_0}	14,088
I_{Z_0}	20,159
Principal axis (relative to thrust line at nose), deg	0.45 up
Center of gravity:	
Location on M.A.C., percent M.A.C.	21.8
Relative to thrust line, percent M.A.C. below	14.8
Wing:	
Span, ft	33.6
Area, sq ft	250
Airfoil section (normal to L. E.):	
Root	Modified 66, 2x–116 (a=0.6)
Tip	Modified 66, 2x–216 (a=0.6)
M.A.C., ft	7.79
Leading edge of M.A.C. (ft behind L. E. root chord)	3.27
Aspect ratio	4.51
Taper ratio	1.84:1.00
Dihedral, deg	0
Sweepback (at quarter-chord line), deg	35
Total area, plain sealed wing flaps, sq ft	12.52
Ailerons:	
Span (along hinge line, each), ft	8.75
Area (rearward of hinge center line, each), sq ft	6.51
Horizontal tail:	
Total area, sq ft	46.53
Vertical tail:	
Fin area (above horizontal tail), sq ft	13.47
Total rudder area, sq ft	10.26
Ventral fin area, sq ft:	
Large ventral	17.10
Small ventral (approx.)	8.50

TABLE II.—TRIM ANGLES OF HORIZONTAL TAIL

Slots (percent span)	δ_f (deg)	Ventral fin	Propeller	Trim C_L	i_t (deg)
0	0	Large	On	0.33 .55 .76	−0.10 −1.10 −2.75
0	40	Large	On	.33 .55 .76 .95	.90 −.60 −1.50 −2.25
40	0	Large	On and off	.33 .55 .76	−.60 −2.70 −4.60
40	40	Large	On	.33 .55 .76 .95	.75 −1.50 −3.20 −4.40
80	0	Large and small	On	.33 .55 .76	0 −2.40 −4.25
80	40	Large	On	.33 .55 .76 .95	.60 −1.40 −3.00 −4.20

TABLE III.—INDEX OF FIGURES

	Figures
Wind-tunnel results:	
Static stability characteristics:	
Longitudinal characteristics	7 and 8
Lateral derivatives	9 and 10
Variations of C_l, C_n, and C_Y with ψ	11
Rolling derivatives:	
Derivatives at ψ=0°	12 and 13
Variations of derivatives with ψ	14
Yawing derivatives:	
Derivatives at ψ=0°	15 and 16
Variation of derivatives with ψ	17
Calculated and flight motions:	
Abrupt deflection and release of rudder	18 to 23
Summary of period and damping values	24
Rudder kicks	25 to 31
Aileron rolls	32 to 35
Nonlinear aerodynamic effects of sideslip	36 and 37

TABLE IV.—FLIGHT CONDITIONS FOR WHICH MOTIONS WERE CALCULATED

Figure	Slots (percent span)	Flaps (deg)	Ventral fin	V_e (mph)	C_L	Type of test
18	40	0	Large	198	0.334	Oscillation
19	40	0	Large	156	.551	Oscillation
20	40	0	Large	136	.759	Oscillation
21	40	40	Large	160	.824	Oscillation
22	40	40	Large	128	.801	Oscillation
23	80	0	Small	120	.977	Oscillation
25	40	0	Small	198	.341	Rudder kick
26	40	0	Small	160	.556	Rudder kick
27	40	0	Small	133	.764	Rudder kick
28	40	0	Small	120	.919	Rudder kick
29	40	40	Large	157	.537	Rudder kick
30	40	40	Large	130	.794	Rudder kick
31	80	0	Small	228	.278	Rudder kick
32	0	0	Small	119	.983	Aileron roll
33	40	0	Small	150	.598	Aileron roll
34	40	40	Large	146	.598	Aileron roll
35	80	40	Small	110	1.169	Aileron roll